

1 The linkage between the warm Arctic and mid-latitude weather and climate is a hot topic for  
2 cryosphere research community and for this reason, I see this study is interesting and worth to  
3 be noticed as a scientific publication. The manuscript is well structured, and the objectives of  
4 this study are clear. The content fits well the scope of ACP.

5 I recommend this manuscript to be published in ACP. However, I see there are some aspects  
6 scientifically and technically that still need further improvement for better clarity of this  
7 manuscript, I hope authors can make corresponding revisions based on my comments below:

8  
9 1 Title: “Revisiting the trend in the occurrences of the “warm Arctic-cold Eurasian continent”  
10 temperature pattern” Why “revisit”? Have you (authors) done this before? Or are there other  
11 papers dealing with this matter before? if so, what are the scientific outcome from those  
12 existing studies?

13 We have not carried out previous research on the potential mechanisms for the trends of  
14 warm-Arctic-cold Eurasian per se, but there have been several other studies that are either  
15 directly or indirectly related to this specific topic. Two main conclusions regarding the  
16 forcing behind the trends stem from these studies. One conclusion is that the recent warm  
17 Arctic-cold continents pattern can be attributable to the Arctic sea ice loss (Inoue et al., 2012;  
18 Tang et al., 2013; Mori et al., 2014; Kug et al., 2015; Cohen et al., 2018; Mori et al., 2019);  
19 The others disputed sea ice loss as a driver for the trend (Blackport et al., 2019; Fyfe, 2019),  
20 Instead, they point to internal atmospheric variability and the Pacific and Atlantic SST  
21 oscillations as potential forcing behind the trends (Lee et al., 2011; Sato et al., 2014;  
22 Matsumura and Kosaka, 2019; Clark and Lee, 2019). Most of these previous studies and the  
23 two school of thought were mentioned in the Introduction. Our work, which took a different  
24 approach, confirmed the second school of thought. Because of these existing studies on this  
25 topic, we used the word ‘revisiting’ in the title of our manuscript.

26  
27 2 To my understanding, SOM is a pure advanced statistical tool and there is nothing related to  
28 the physics, right? If this is the case, shall I say any results come from SOM have  
29 uncertainties because you need to pre-define SOM nodes and this procedure is a kind  
30 arbitrary, right? On top of it, as you pointed out in the abstract only 40% of the surface  
31 temperature trends are explained by SOM pre-defined nodes that fit to your pre-condition, i.e.  
32 warm Arctic-cold Eurasian continent. What I am trying to say is that for what kind of criteria  
33 you need to be satisfied before you can make a rebuts conclusion to say: “ok, there is a  
34 linkage” or “no, there isn’t a linkage”. This comment and “a kind of arbitrary” above come  
35 from your description on line 141-143.

36 SOM is an advanced statistical tool for pattern extraction. Although SOM is superior to some  
37 other existing pattern extraction tools such as EOF, it suffers from the same limitations as  
38 other statistical tools in identifying physical modes. That was why a large part of the  
39 manuscript was devoted to explain the existence of the patterns and their trends based on  
40 physical understanding of atmosphere and ocean dynamics that had been established from  
41 theoretical framework and/or from coupled ocean-atmosphere modeling. Yes, to use the SOM  
42 method, one has to pre-define SOM nodes and the procedure is not completely objective. A  
43 small grid (each node has larger frequency of occurrence) tends to miss transitions between  
44 the main patterns that are retained by a large grid. But an excessively large grid could

45 sidetrack the attention from the main variability patterns. Nevertheless, changing the grid  
46 from 3x3 to 4x4 or even larger would not change the main conclusion.

47

48 3 How sensitivity of the data source will impact the final result? In this study, you have  
49 applied ERA-Interim data. if you use other data resource, e.g. NCEP or MERRA, would be  
50 your conclusion changed entirely or partly? I am not asking to use these data sets to rerun  
51 SOM, but it would be nice to comment it at the end of this study.

52 We believe our results are not particularly sensitive to the specific large-scale reanalysis data  
53 source. We could have also used ERA5, or NCEP or MERRA and arrived at similar  
54 conclusions, although there might be some minor differences. We have added some  
55 comments on this point at the end of the study.

56

57 4 Authors focused on the impacts of the SST anomalies over North Pacific and Atlantic  
58 Oceans on the trend in the occurrences of the “warm Arctic cold Eurasian continent”  
59 temperature pattern. The influence of decreasing Arctic sea ice cannot be ignored.

60 You may consider to add discussions on the influence of sea ice to your pre-defined warm  
61 Arctic and cold Eurasian content.

62 We added some discussions on the influence of sea ice in the Conclusions and Discussions  
63 section.

64

65 There are a number of technical details need to be clarified:

66 a) Fig.1: All “percent” sum together is larger than 100%, please check.

67 Changed

68

69 b) Fig.2: The color bar refers to what? Contour color? what are the background (fingerprint  
70 like) information in each sub-plot? The text explanation for figure 2 (line 182 -185) and figure  
71 2 presentation seems not match to each other. I suggest you remove unnecessary from the plot  
72 and only show what you have explained in the text so readers can understand better.

73 Both color bar and contour color refer to 500-hPa geopotential height anomalies. Dotted  
74 regions in each sub-plot indicate the above 95% confidence level.

75 We revised some of the discussion.

76

77 c) The comment above applied to at least Fig, 3, 4, 5 and 6.

78 In Figure 3-6, shaded and dotted regions indicate the above 95% confidence level.

79

80 d) “same as Figure2, but for,,,” This is not a good figure caption, please write clear with full  
81 information. For those surface fluxes, I think you need to explain the unit of the fluxes, are  
82 those daily accumulated fluxes?

83 We revised figure caption with details. The fluxes are daily accumulated fluxes, which are  
84 now explained in the caption and text.

85

86 e) The sea ice concentration figure needs more explanations, e.g. node information was  
87 missing; what was meant for positive and negative anomalous? is this also for winter season?  
88 how about summer season? Now I realized you actually only investigate winter season for

89 everything, if so, you need to say this explicitly in the beginning of the paper.  
90 We added node information. The anomalous sea ice concentration is a composite result based  
91 on the occurrences of nodes. For example, the negative sea ice concentration corresponds to  
92 the spatial pattern of air temperature for node 1. In this paper, we only examine warm  
93 Arctic-cold continents pattern in boreal winter, which was mentioned in the first and second  
94 paragraph of the manuscript.  
95  
96 f) Fig.7 and 14: I have difficult to understand these figures? What we can learn from those  
97 figures? If you only tell the integrated total number of days for each node and compared with  
98 showing this figure, what we will missing up?  
99 Figure 7 and 14 show the integrated total number of days for each node. In Figure 7 and 14,  
100 the numbers for nodes 1 and 4 are larger after 2000 than those prior to 2000. The opposite  
101 occurs for nodes 6 and 9. Figure 14 mainly show an interdecadal variability of the number.  
102 The trends in the number for nodes 1, 4, 6, and 9 are a fragment of the interdecadal variability.  
103 We added clarification in the discussion.  
104  
105 g) Fig. 12: “wave activity flux”: This need to be explained more in detail both here and in the  
106 text. 100m<sup>2</sup>/s, what is this? and in the caption:107 m<sup>2</sup>/s.  
107 “vector 100m<sup>2</sup>/s” in the figure is figure legend of wave activity flux. The unit of stream  
108 function is m<sup>2</sup>/s and its magnitude is the product of the values in the figure and 10<sup>7</sup>. We have  
109 added explanation of wave activity flux in the discussion and in the figure caption with a  
110 reference.  
111  
112 h) Please mark the study area in corresponding figures 2-6, to help readers understand the  
113 mechanism impact more intuitively.  
114 Marked  
115  
116 i) Table 3 is not mentioned in the article, and some problems of uppercase and lowercase  
117 letters (such as not show or Not show), please check them carefully.  
118 Changed  
119  
120 j) The order of the nodes should be consistent in figures, 10-12.  
121 Changed  
122  
123 k) Authors should increase some discussions about the application of statistical results in  
124 prediction of surface temperature Arctic cold Eurasian continent.  
125 Added discussion  
126  
127 The results in this study are based on statistical analysis. Some numerical experiments may be  
128 considered in the further studies.  
129 Added  
130  
131  
132

133 General comments

134 The description of the SOM and the transition between nodes is good.

135 Please refer to figures more throughout the results section. I'd cite the figure number each  
136 time you change which figure you are discussing. For example, on line 230 you mention  
137 Figure 6, but then in the following line you are referring to Figure 5 but you do not give the  
138 figure number. It would be easy here (and in other places) for the reader to be looking at the  
139 wrong figure. The paragraph starting at line 277 is another instance where figures should be  
140 referred to more frequently.

141 **Good suggestion. We have gone through the manuscript carefully and added citations to**  
142 **figures whenever appropriate.**

143

144 Datasets and methods section – this section provides a good explanation of SOMs, including  
145 what SOMs are and how you will apply them to temperature data, but there is no explanation  
146 of how you analyse the other variables (i.e. create composites based on the SOM for  
147 temperature data), or the use of principal component analysis. Please include this here.

148 **Thanks for pointing out this oversight. We have added more description about the other**  
149 **methods we also used in the analyses, in addition to SOM, in the Method section.**

150

151 Consider adding analysis to show what portion of the trend in the warm Arctic-cold

152 Eurasia pattern is due to mean warming. What trend is removed from the 20CR data?

153 It seems an oversight to not consider mean warming when so many other variables are being  
154 examined.

155 **Trend in wintertime surface air temperature anomalies for the 1854-2014 period for the 20CR**  
156 **data was removed.**

157 **In this study, we mainly focused on the role of the interdecadal variability of SST anomalies**  
158 **over northern oceans in trend in the warm Arctic-cold Eurasia pattern. In Conclusions and**  
159 **Discussions section, we increased some discussions of the role of Arctic warming in the**  
160 **trend.**

161 Specific comments

162 Lines 23-36 – Abstract nicely sums up the major findings of the paper.

163 **Thanks**

164 Line 53 – This line states that the warm Arctic-cold continents pattern has been observed on  
165 an interannual timescale. Please state here whether the pattern has been strengthening linearly  
166 over time, or whether it's a cyclical pattern, or something else.

167 **We have added a statement here about increasing trend in the occurrence of the warm**  
168 **Arctic-cold continents pattern.**

169 Line 75 – What changes in the Gulf Stream are you referring to here?

170 **Changed the statement to "... the sea surface temperature anomalies over the Gulf Stream."**

171 Line 85 – "Using regression method" should probably read "using regression", or "using  
172 linear regression" (if this is correct).

173 **Changed to 'using linear regression'**

174 Lines 90-98 – This first part of the Datasets and methods section seems to be replicating some  
175 of what is said in section 2.2. I'd suggest starting the datasets and methods section with  
176 section 2.1, and incorporating lines 90-98 into section 2.2.

177 **Removed the replications**

178 Line 94 – Should this say “41 winters”? Or are you only considering complete winters, i.e.  
179 December 1979-February 2019 (thus excluding January and February 1979, and  
180 December 2019)? Which months do you use for winter? I assume it’s DJF.  
181 **Winter is defined by DJF and we only consider complete winters from December 1979**  
182 **through February 2019. This is now clarified.**

183 Line 102 – What is the resolution of the ERA-Interim data?  
184 **The resolution of the ERA-Interim was added.**

185 Lines 137-138 – What dataset are these lines referring to? Both ERA-Interim and  
186 20CR? If both, which 40-year period do you use? I.e. do you subtract the 1979-2019 mean  
187 from both datasets?  
188 **These lines refer to ERA-Interim reanalysis. We subtract the 1979-2019 mean from**  
189 **ERA-Interim.**

190 Line 150 – Do the SOM-explained trends mean something physically, i.e. are they the  
191 fraction of the total trends that are explained by changes in circulation (or something else)?  
192 **The SOM-explained trends are the fraction of the total trends that are explained by the**  
193 **changes in circulations.**

194 Lines 161-162 – This sentence compares the “first node” in each group, however node  
195 9 appears to be the second node in group one, and node 1 is the first node in group two.  
196 **Changed**

197 Lines 164-165 – It is not clear from Figure 1 that the maximum anomalies are centered near  
198 Svalbard. Please consider adding contour lines to the SOMs, or use a discrete color scale.  
199 When you say maximum, are you referring to the greatest departure from zero (i.e. positive or  
200 negative values)?  
201 **Contour lines are added. Maximum refers to largest values of the anomalies**

202 Line 165 – This line states that nodes 3 and 7 are the second most frequently occurring of  
203 their groups, but node 3 occurs most frequently. The comparison of pairs is good, but needs to  
204 be worded more carefully. Maybe pick the most frequently occurring node in group 1 then  
205 identify its pair.  
206 **Good suggestion. Statements rephrased.**

207 Lines 171-172 – Why can’t this SOM consider temperature trends? I think this should say  
208 “does not” not “cannot”.  
209 **Changed to “does not”**

210 Lines 176-180 – Consider moving these lines to the methods section.  
211 **We have added some description on composite method in the Method section, following**  
212 **another reviewer’s comment.**

213 Line 193 – Please add figure reference.  
214 **Referred more to figures whenever appropriate.**

215 Line 223 – Nice explanation of turbulent heat flux!  
216 **Thanks**

217 Line 229 – Maybe refer back to Figures 2 and 3 if that is where this statement comes from.  
218 **Made references back to the figures**

219 Lines 229-230 – Are you sure this is the correct order? I.e. over the Barents Sea in node 1, is  
220 it possible that the sea ice melt causes a reduction in the albedo which results in an increased

221 turbulent heat flux?  
222 We believe the cause-effect is correct based on previous studies (Blackport et al., 2019)  
223 Line 231 – When you say “larger” do you mean larger spatially, or a greater magnitude  
224 anomaly?  
225 A greater magnitude anomaly. Clarified  
226 Line 238 – “composted” should probably be “composited”.  
227 Changed  
228 Line 239 – What happens if you do the same lag analysis for sea ice concentration? I think it  
229 is important to know that sea ice does not also peak before the day the nodes occur. Similarly,  
230 what happens if you do this lag analysis on the geopotential height patterns?  
231 It seems strange to say that circulation leads sea ice cover without mentioning the  
232 geopotential height patterns.  
233 The pattern of the composited anomalous 500-hPa geopotential height, turbulent heat flux,  
234 and sea ice concentration 2 days prior to the day when the nodes occur (not shown) is similar  
235 to the simultaneous pattern in Figures 2, 5, and 6.  
236 Lines 250-251 – How does this differ to the other nodes? I assume they only exhibit  
237 interannual variability.  
238 The main difference is the decadal variability.  
239 Line 255 – I think this should refer to Table 3 (not Table 2).  
240 Changed  
241 Line 261 – Figure 8 does not appear to cover a large enough region to determine whether  
242 there are positive trends over southern Europe. This might need re-wording.  
243 Rewording done  
244 Line 262 – Maybe point out that negative trends are mostly not significant.  
245 Done  
246 Line 267 – Arctic-cold should be Arctic-cold  
247 Changed  
248 Line 281 – Refer to figure number (Figure 11).  
249 Added reference to Figure 11  
250 Lines 282-285 – Which node are you referring to? I assume node 1 but this should be clear.  
251 Added reference to node 1.  
252 Lines 284-285 – Are you determining the direction of propagation from Figure 11 or Figure  
253 12? From the text it sounds like you are only referring to Figure 11, but I am not sure how  
254 you are determining that the Rossby wave moves southeastwards to the Eurasian continent  
255 from this figure. Please explain and give figure number.  
256 The direction of wave activity flux points to the Eurasian continent (Figure 12). A reference  
257 to Figure 12 is added.  
258 Lines 285-286 – What figure(s) support the claim that “large SST anomalies over the  
259 Nordic Ocean augment the wave signal through local air-sea interaction”? This statement  
260 needs more support and/or more of a description on how you came to this conclusion.  
261 Added more descriptions with reference to figures  
262 Line 290 – Figure number?  
263 Added  
264 Line 302 – Does “these results” refer to the results in Figures 10-12, or to the results you just

265 mentioned in lines 299-302? If you're referring to Figures 10-12, please state this.  
266 **Reference to Figures 10-12 are added**  
267 Line 308 – Which figure are you referring to here? If this comparison is not shown, write  
268 “(not shown)”.  
269 **“(not shown)” was added.**  
270 Line 321 – Where it states that the magnitude is smaller for the 20 CR data, could this be  
271 because the 20 CR data are detrended and the ERA-Interim data are not?  
272 **Added detrending of the 20CR as a potential explanation**  
273 Lines 321-322 – This sentence says “frequencies of all the nodes (Figure 14)”, but Figure 14  
274 only shows data for nodes 1, 4, 6, and 9 – please rectify.  
275 **Clarified**  
276 Line 322 – Please refer to the corresponding figure that shows node occurrence for  
277 ERA-Interim.  
278 **Reference to corresponding figures added**  
279 Line 325 – The occurrence frequencies at the end of the time series in node 1, Figure 7,  
280 appear to be slightly greater than those for node 1 in Figure 14. Could this indicate that mean  
281 warming amplifies these trends?  
282 **Global warming may be a reason**  
283 Lines 335-336 – If these results are not shown, please state this.  
284 **Stated**  
285 Lines 343-344 – Why isn't the central North Pacific Ocean SST index shown in Figure  
286 15 since it is significantly correlated with EOF modes 1 and 2?  
287 **The central North Pacific Ocean SST index is added in Figure 15**  
288 Line 347 – And the PDO?  
289 **Added**  
290 Lines 386-387 – Which figures are you referring to here?  
291 **References to corresponding figure added**  
292 Lines 388-389 – How does this atmospheric process suggest that the relationship between a  
293 warmer Arctic and East Asian cold spells are not as strong? If the atmospheric patterns  
294 described by your SOMs show changes in circulation patterns lead to increases in Arctic  
295 temperatures and decreases in Eurasian temperatures, then there appears to be a strong link.  
296 Or are you saying that temperature increases in the Arctic are not the driver of temperature  
297 decreases in Eurasia?  
298 **Temperature increases in the Arctic are not the driver of temperature decreases in Eurasia.**  
299  
300 **Figures**  
301 In general - Please add the following to the figure captions: - What years the figure covers (if  
302 not shown). E.g. Figure 1 - Whether the data have been detrended or not -  
303 Dataset used - Consider making figures more consistent, for example, Figure 10 has the  
304 Pacific Ocean in the center, whereas Figure 12 has the Atlantic in the center. It would be  
305 easier to compare these figures if they both had the same east/west bounds.  
306 **Years and data were added in figure captions. Figure 10 has changed.**  
307 Figure 1 - Please consider adding contour lines to the SOM, or use a discrete color scale so it  
308 is clearer where the maximum/minimum values are on these plots. – Please mention years and



309 dataset in the caption.

310 **Figure 1 has been changed into contour lines.**

311 Figure 2 - Please reconsider the use of a rainbow color scale. Reds and greens can look  
312 identical to color blind people. - It appears that the stippling/hatching is plotted on top of the  
313 contour lines. The plot might be easier to read if the contour lines were on top of the  
314 stippling/hatching. - The caption states that this is the “corresponding 500-hPa  
315 geopotential height anomalies”, but you do not mention that it corresponds to Figure  
316 1. - The caption states that stippled areas are significant, but what about the hatched areas? I  
317 assume they are also significant. - Please mention what contour lines show in caption. -  
318 Maybe consider rotating the nodes so they match Figure 1 better, i.e. put Russia at the bottom  
319 of the subplots. Alternatively, adding an outline of the region in Figure 1 to the plots like  
320 Figure 2 would be helpful.

321 **Rainbow color scale is now used. An outline of the region in Figure 1 is added. We used  
322 stippled, not hatched in Figure 2.**

323 Figure 3 - It would be useful to show the contour lines (from Figure 2) on this plot as well  
324 (without stippling) so we can see exactly how the contour lines and wind anomalies line up. -  
325 What does the gray shading mean?

326 **Adding contour lines made it harder to see vectors. We replaced stippling by shading to denote  
327 the above 95% confidence level.**

328 Figure 6 - Node numbers are missing from Figure 6. Please add them.

329 **Added**

330 Figure 7 - Consider adding trend lines and p-values to each subplot (and other similar  
331 figures).

332 **Added**

333 Figures 10, 11, and 12 - Consider arranging these plots the same, i.e. all 2x2 or 1x4 for easier  
334 comparison between the figures.

335 **Rearranged**

336 Figure 14 - Can the results from Figure 7 be overlaid on Figure 14? Maybe with gray dashed  
337 outlines. This would make it clearer to see the similarities/differences between the results.

338 **The time series in Figure 7 is added in Figure 14**

339 Figure 15 - Consider putting r and p values on subplots b and d. Or in caption.

340 **R and P values are added in the caption**

341

342

343

344

345

346



347 **Revisiting the trend in the occurrences of the “warm Arctic-cold Eurasian continent”**

348 **temperature pattern**

349 Lejiang Yu<sup>1,2\*</sup>, Shiyuan Zhong<sup>3</sup>, Cuijuan Sui<sup>4</sup>, and Bo Sun<sup>1</sup>

350 1MNR Key Laboratory for Polar Science, Polar Research Institute of China, Shanghai, China

351 2 Southern Marine Science and Engineering Guangdong Laboratory (Zhuhai), Zhuhai, Guangdong,

352 China

353 3Department of Geography, Environment and Spatial Sciences, Michigan State University, East

354 Lansing, MI, USA

355 4 National Marine Environmental Forecasting Center, Beijing, China

356

357 \*Corresponding Author’s address

358 Dr. Lejiang Yu

359 MNR Key Laboratory for Polar Science, Polar Research Institute of China

360 451 Jinqiao Rd. Shanghai, 200136

361 Phone: 86-21-58712034,

362 Email: yulejiang@sina.com.cn

363

364

365

366

367

368

369 **Abstract.** The recent increasing trend of “warm Arctic, cold continents” has attracted much attention,  
370 but it remains debatable as to what forces are behind this phenomenon. Here, we revisited  
371 surface-temperature variability over the Arctic and Eurasian continent by applying the  
372 Self-Organizing-Map (SOM) technique to gridded daily surface temperature data. Nearly 40% of the  
373 surface temperature trends are explained by the nine SOM patterns that depict the switch to the current  
374 warm Arctic-cold Eurasia pattern at the beginning of this century from the reversed pattern that  
375 dominated the 1980s and the 90s. Further, no cause-effect relationship is found between the Arctic  
376 sea-ice loss and the cold spells in high-mid latitude Eurasian continent suggested by earlier studies.  
377 Instead, the increasing trend in warm Arctic-cold Eurasia pattern appears to be related to the anomalous  
378 atmospheric circulations associated with two Rossby wavetrains triggered by rising sea surface  
379 temperature (SST) over the central North Pacific and the North Atlantic Oceans. On interdecadal  
380 timescale, the recent increase in the occurrences of the warm Arctic-cold Eurasia pattern is a fragment  
381 of the interdecadal variability of SST over the Atlantic Ocean as represented by the Atlantic  
382 Multidecadal Oscillations (AMO), and over the central Pacific Ocean.

383

384 **Key words:** Warm Arctic-cold Eurasian continent, Arctic Sea ice, the Kara-Barents Sea, the  
385 Self-Organizing-Map (SOM), the Pacific Decadal Oscillation (PDO), the Atlantic Multidecadal  
386 Oscillation (AMO)

387

388

389

390

391 **1 Introduction**

392 In recent decades, winter season temperature in the Arctic has been rising at a rate faster than the  
393 warming experienced in any other regions of the world (Stroeve et al., 2007; Screen and Simmonds,  
394 2010; Stroeve, 2012). In contrasts, there has been an increasing trend in colder than normal winters  
395 over the northern mid-latitude continents (Mori et al., 2014; [Cohen et al., 2014; 2018](#)). This pattern of  
396 opposite winter temperature trend between the Arctic and high-mid latitude continents, referred to as  
397 the warm Arctic-cold continents pattern (Overland et al., 2011; Cohen et al., 2014; Walsh, 2014), has  
398 ~~also been observed on the interannual timescale~~[received considerable interest in the scientific](#)  
399 [community especially with regard to dynamical and physical mechanisms for the development of the](#)  
400 [phenomenon](#) (Mori et al., 2014; ~~Kug et al., 2015~~)~~The question as to what processes are responsible for~~  
401 ~~the opposite change of winter air temperature between the Arctic and mid latitudes remain open~~  
402 (~~Vihma, 2014; Barnes and Screen, 2015; Kug et al., 2015; Overland et al., 2015; Chen et al., 2018~~).

403 [Using observational analyses or coupled ocean-atmosphere modeling](#), ~~A~~ number of studies have  
404 attributed the recent warm Arctic-cold continents pattern to the Arctic sea ice loss [in boreal winter](#)  
405 (Inoue et al., 2012; Tang et al., 2013; Mori et al., 2014; Kug et al., 2015; Cohen et al., 2018; Mori et al.,  
406 2019). Sea ice variability in different parts of the Arctic Ocean has been linked to climate variability in  
407 different parts of the world. Specifically, sea ice loss in the Barents and Kara Seas has been linked to  
408 cold winters over East Asia (~~add a reference~~ [Kim et al., 2014; Mori et al., 2014; Kug et al., 2015;](#)  
409 [Overland et al., 2015](#)) [and in central Eurasia \(Mori et al., 2014\)](#), while a similar connection has been  
410 found between cold winters in North America and sea ice retreat in the East Siberian and Chukchi Seas  
411 (Kug et al., 2015). A most recent study (Matsumura and Kosaka, 2019) attributed the warm Arctic-cold  
412 continents pattern to the combined effect of Arctic sea ice loss and the atmospheric teleconnection

413 induced by tropical Atlantic sea-surface temperature (SST) anomalies. ~~Some recent studies have~~  
414 ~~suggested that the mid-latitude atmospheric circulation anomalies play a role in the formation of the~~  
415 ~~warm Arctic-cold continents pattern (Luo et al., 2016; Peings et al., 2019).~~

416 Other studies, however, found no cause-and-effect relationship between Arctic sea ice loss and  
417 mid-latitude climate anomalies (Blackport et al., 2019; Fyfe, 2019). Numerical modeling studies using  
418 coupled ocean and atmospheric models simulated no cold mid-latitude winters when the models were  
419 forced with reduced Arctic sea ice cover (McCusker et al., 2016; Sun et al., 2016; Koenig et al., 2019;  
420 Blackport et al., 2019; Fyfe, 2019). ~~Instead, The results from~~ these studies pointed to internal  
421 atmospheric variability as the likely cause for cold winters in mid-latitudes. Some studies have also  
422 suggested that on the interannual timescale mid-latitude atmospheric circulation anomalies triggered by  
423 the Pacific and Atlantic SST oscillations may explain both the Arctic sea ice loss and the cooling of the  
424 high-mid latitudes (Lee et al., 2011; [Luo et al., 2016](#); [Peings et al., 2019](#); Matsumura and Kosaka, 2019;  
425 Clark and Lee, 2019). The [sea surface temperature anomalies over the](#) Gulf Stream ~~have~~ ~~has~~ also been  
426 linked to the Barents Sea ice loss and Eurasian cooling (Sato et al., 2014).

427 Despite the recent attention given to the warm Arctic-cold continents pattern, it remains debatable  
428 as to ~~what the roles of various dynamical and physical processes play may be responsible in the~~  
429 ~~formation of~~ ~~for~~ this phenomenon. In this study, we revisit surface temperature variability over the  
430 Arctic and Eurasia continent (40-90°N, 20-130°E), where the warm Arctic-cold continents pattern is a  
431 prominent feature (Cohen et al., 2014; Mori et al., 2014), by applying the Self-Organizing-Map (SOM)  
432 technique to daily surface temperature over the recent four decades. We will show that while the warm  
433 Arctic-cold Eurasian continent pattern has dominated the recent two decades, its opposite pattern, cold  
434 Arctic-warm Eurasia continent, appeared frequently in the 1980s and the 90s. Using century-long data,

435 we will further show that the warm Arctic-cold Eurasian continent pattern is an intrinsic climate mode  
436 and the recent increasing trend in its occurrence is a reflection of an interdecadal variability of the  
437 pattern. Using [linear](#) regression ~~method~~, we explain the reason for the recent increasing occurrences of  
438 the warm Arctic-cold continents pattern. We also assess the role of the SST anomalies over the North  
439 Pacific and Atlantic Oceans in the variability of the warm Arctic-cold Eurasia pattern on the  
440 interdecadal time scale.

## 441 2 Datasets and methods

~~442 From the perspective of nonlinear dynamic, a region's climate has its intrinsic modes of variability, but  
443 the frequency of occurrence of these internal modes can be modulated by remote forces external to the  
444 region (Palmer, 1999; Hoskins and Woollings, 2015; Shepherd, 2016). In this study we will first obtain  
445 the main modes of variability of wintertime surface temperature in a region (40-90 N, 20-130 E) by  
446 applying the SOM method (Kohonen, 2001) to daily surface temperature data for the 40 winters in the  
447 1979-2019 period. The use of daily data over four decades allows for capturing the variability across  
448 two time scales (synoptic and decadal). We will then determine, through regression and composite  
449 analyses, the relationships of these modes of climate variability of surface air temperature to known  
450 climate variability modes at corresponding time scales.—~~

### 451 2.1 Datasets

452 Daily surface air temperature and other climate variables used in the current analyses, including  
453 500 hPa geopotential height, 800-hPa wind and mean sea level pressure, all come from the [European](#)  
454 [Centre for Medium-Range Weather Forecasts Re-Analysis \(ERA\)](#), the interim version (ERA-Interim;  
455 [Dee et al., 2011](#)) [with a horizontal resolution of approximately 79 km \(T255\) and 60 vertical levels in](#)  
456 [the atmosphere](#). Compared to the earlier versions of ERA (e.g., ERA-40, Uppala et al., 2005) and other

457 global re-analysis products (e.g. the NCEP reanalysis, Kalnay et al., 1996), ERA-Interim has been  
458 found to be more accurate in portraying the Arctic warming trend (Dee et al., 2011; Screen and  
459 Simmonds, 2011) despite its known warm and moist bias in the surface layer (Jakobson et al., 2012).

460 Daily sea ice data are obtained from the U.S. National Snow and Ice data Center  
461 ([ftp://sidacs.colorado.edu/DATASETS/nsidc0051\\_gsfc\\_nasateam\\_seaice/final-gsfc/north/daily](ftp://sidacs.colorado.edu/DATASETS/nsidc0051_gsfc_nasateam_seaice/final-gsfc/north/daily)).

462 Gridded monthly SST data used in the current analysis are obtained from the U.S. National Oceanic  
463 and Atmospheric Administration (NOAA) data archives  
464 (<ftp://ftp.cdc.noaa.gov/Datasets/noaa.oisst.v2.highres/>) (Reynolds et al. 2007).

465 The results obtained from the data within the recent four decades are put into the context of the  
466 variability over longer time scales using data from the Twentieth Century Reanalysis project, version  
467 2Ce (20CR) that spans more than a century from 1851 through 2015 (Compo et al., 2011). The 20CR  
468 reanalysis data, which has a horizontal resolution of 2 °latitude by 2 °longitude and temporal resolution  
469 of 6 hours. ~~Through the assimilation of surface observational pressure data, the 20CR reanalysis~~ was  
470 produced by ~~the~~ model ~~whose driven at the~~ lower boundary ~~by condition is derived from observed~~  
471 monthly SST and sea ice conditions and with data assimilation of surface pressure observations.  
472 ~~Various~~ Several indices used to describe known modes of climate variability ~~are obtained from~~  
473 ~~NOAA's Climate prediction Center (CPC) (<https://www.esrl.noaa.gov/psd/data/climateindices/list/>),~~  
474 ~~which~~ including Arctic oscillation (AO), Northern Atlantic Oscillation (NAO), Atlantic Multidecadal  
475 Oscillation (AMO) (Enfield et al., 2001) and PDO (Mantua et al., 1997) ~~indices.~~ are obtained from  
476 NOAA's Climate prediction Center (CPC) (<https://www.esrl.noaa.gov/psd/data/climateindices/list/>).

## 477 2.2 Methods

478 From the perspective of nonlinear dynamic, a region's climate has its intrinsic modes of variability.

479 but the frequency of occurrence of these internal modes can be modulated by remote forces external to  
480 the region (Palmer, 1999; Hoskins and Woollings, 2015; Shepherd, 2016). In this study we will first  
481 obtain the main modes of variability of wintertime surface temperature in a region (40-90°N, 20-130°E)  
482 by applying the SOM method (Kohonen, 2001) to daily surface temperature data for the 40 winters  
483 (December, January, -February) in the 1979-2019 period from December 1979 through February 2019.  
484 The use of daily data over four decades allows for capturing the variability across two time scales  
485 (synoptic and decadal). ~~The 40-year, daily surface temperature over the study region (40-90°N,~~  
486 ~~20-130°E) is decomposed using the SOM method.~~ SOM is a clustering method based on neural  
487 network that can transform multi-dimensional data into a two-dimensional array without supervised  
488 learning. The array includes a series of nodes arranged by a Sammon map (Sammon, 1969). Each node  
489 in the array has a vector that can represent a spatial pattern of the input data. The distance of any two  
490 nodes in the Sammon map represents the level of similarity between the spatial patterns of the two  
491 nodes. Because SOM has fewer limitations than most other commonly used clustering methods, (e.g.,  
492 orthogonality required by the empirical orthogonal function or EOF method ), the SOM method can  
493 describe better the main variability patterns of the input data (Reusch et al., 2005).

494 SOM method has been used in atmospheric research at mid and high latitudes of the northern  
495 hemisphere (Skific et al., 2009; Johnson and Feldstein, 2010; Horton et al., 2015; Loikith and Broccoli,  
496 2015; Vihma et al., 2019). For example, Johnson and Feldstein (2010) used SOM to identify~~ied the~~  
497 spatial patterns of ~~the~~ daily wintertime North Pacific sea level pressure and related ~~the~~ the variability of the  
498 occurrences of those patterns to some large-scale circulation indices. Loikith and Broccoli (2015)  
499 compared observed and model-simulated circulation patterns across the North American domain using  
500 an approaching involving SOM. The SOM method was also used to detect circulation pattern trends in



501 a subset of North America during two [different](#) periods (Horton et al., 2015).  
502 In this study, the SOM method is applied to [ERA-Interim](#) wintertime daily temperature anomalies [from](#)  
503 [December 1979 through February 2019. The anomalies are calculated](#)~~obtained~~ by subtracting 40-year  
504 averaged daily temperature from the original daily temperature at each grid point. Prior to SOM  
505 analysis, it is necessary to determine how many SOM nodes are needed to best capture the variability  
506 in the data. According to previous studies (Lee and Feldstein, 2013; Gibson et al., 2017; Schudeboom  
507 et al., 2018), the rule for determining the number of SOM nodes is that the number should be  
508 sufficiently large to capture the variability of the data analyzed, but not too large to introduce  
509 unimportant details. Table 1 shows the averaged spatial correlation between all daily surface air  
510 temperature [anomalies](#) and their matching nodes. ~~There is an increase in~~ [The spatial](#) correlation  
511 coefficients [increase](#) from 0.26 for a 3×1 grid to 0.51 for a 4×4 grid, but the gain from a 3×3 grid to a  
512 4×4 grid is relatively small. Hence, a 3×3 grid seems to meet the above-mentioned rule and will be  
513 utilized in this study.

514 The contribution of each SOM node to the trend in wintertime surface temperature [anomalies](#) is  
515 calculated by the product of each node pattern and its frequency trend normalized by the total number  
516 [\(90\)](#) of wintertime days ~~(90,~~ Lee and Feldstein, 2013). The sum of the contributions from all nodes  
517 denotes the SOM-explained trends. Residual trends are equal to the subtraction of SOM-explained  
518 trends from the total trends. [The anomalous atmospheric circulation pattern corresponding to each of](#)  
519 [the SOM pattern is obtained by composite analysis that computes a composite mean of an atmospheric](#)  
520 [circulation field \(e.g., 500 hPa height\) over all occurrences of that SOM node. Regression analysis is](#)  
521 [also performed where atmospheric circulation variables are regressed onto the time series of the](#)  
522 [occurrence of a SOM node to further elucidate the relationship between the variability of atmospheric](#)

523 [circulations and surface temperatures](#). The statistical significance [of composite and regression analyses](#)  
524 in this study is tested by using the Student's t test.

### 525 **3 Results**

#### 526 3.1 Surface temperature variability

527 The majority of the 9 SOM nodes depict a dipole pattern characterized by opposite changes in  
528 [surface temperatures](#) between the Arctic Ocean and the Eurasian continent, although the sign switch  
529 does not always occur at the continent-ocean boundary (Figure 1). The [differences in the](#) position of the  
530 boundary between the warm and cold anomalies [reflects](#) the transition between the cold Arctic-warm  
531 Eurasia pattern (denoted, in descent order of the occurrence frequency, by nodes 3, 9, 6), to the warm  
532 Arctic-cold Eurasia pattern (depicted, in descent order of the occurrence frequency, by nodes 1, 7, 4).

533 The spatial patterns represented by the first group of nodes (~~3, 9, 6~~) are almost mirror images of the  
534 patterns denoted by the corresponding nodes in the second group (~~1, 7, 4~~). For example, the [first-second](#)  
535 node in group 1 (node 9, 15.4%) and [the first node](#) in group 2 (node 1, 17.1%) show a mirror image  
536 pattern with cold (warm) anomalies in the Arctic Ocean extending into northern Eurasia and warm  
537 (cold) anomalies in the rest of the Eurasia continent in the study domain. In both cases, the region of  
538 maximum [anomalies-magnitude anomalies](#) is centered near Svalbard, Norway. The second ~~most~~  
539 [frequent-patternpair](#), denoted by node 3 (17.2%) and 7 (13.7%) ~~in the two groups, respectively~~, has the  
540 boundary of separation moved northward from northern Eurasia continent toward the shore of the  
541 Arctic Ocean. While the maximum anomaly in the Arctic Ocean remains close to Svalbard, maximum  
542 values over the continent are found in central Russia. Nodes 4-6 display a noticeable transition from  
543 node 1 to node 7 and from node 3 to node 9, respectively. Although nodes 2 and 8 show an  
544 approximate monopole spatial pattern, they also represent a transition between nodes 1 and 3, and

545 between nodes 7 and 9, respectively. Above SOM analysis ~~cannot~~does not consider the trend in surface  
546 air temperature. The result is similar ~~while when removing~~ the trend is removed (~~Not-not~~ shown).

547 The temporal variability on this time scale is typically related to synoptic processes and hence the  
548 questions are what synoptic patterns are responsible for the occurrence of the spatial patterns depicted  
549 by each of the 9 SOM nodes and how these patterns are related to those of the Arctic sea ice anomalies?

550 These questions can be answered by using the composite method. Specifically, for each SOM node,  
551 composite maps are made respectively for the anomalous 500-hPa geopotential height, mean sea level  
552 pressure, 850-hPa wind, downward longwave radiation, surface turbulent heat flux, and sea ice  
553 concentration over all the days when the spatial variability of the surface temperature anomalies is best  
554 matched by the spatial pattern of that node.

### 555 3.2 Large-scale circulation patterns

556 For all SOM nodes, the spatial pattern of the composited 500 hPa-geopotential height anomalies  
557 (Figure 2) is similar to that of mean sea level pressure anomalies (~~Not-not~~ shown), indicating an  
558 approximately barotropic structure. For nodes 1, 4 and 7, the 500-hPa height anomalies show a dipole  
559 structure of positive values over Siberia and negative values to its south over the Eurasian continent.

560 Anomalous southwesterly winds on the western side of the anticyclone over Siberia transport warm  
561 and moist air from northern Europe and the North Atlantic Ocean into the Atlantic sector of the Arctic  
562 Ocean (Figure 3), providing a plausible explanation of the warm surface temperature anomalies in the  
563 region (Figure 1). On the eastern side of the anticyclone, anomalous northwesterly winds bring cold  
564 and dry air from the Arctic Ocean into Eurasia continent, which is consistent with the negative surface  
565 temperature anomalies there. The opposite occurs for nodes 3, 6 and 9. A similar explanation involving  
566 anomalous pressure and wind fields can be applied to other nodes. The dipole structure that dominates

567 the anomalous 500-hPa height fields over the North Atlantic Ocean for most nodes resembles the  
568 spatial pattern of the NAO (Figure 2). In addition, the patterns for ~~several~~ a few nodes, such as nodes 4  
569 and 7, have some resemblance to the spatial pattern of the AO over larger geographical region. The  
570 possible connection to NAO and AO is further investigated by averaging the daily index values of  
571 NAO or AO over all occurrence days for each node. The results (Table 2) show that nodes 1, 2, 3 (5, 8,  
572 9) correspond to a significant positive (negative) phase of the NAO index characterized by negative  
573 (positive) height anomalies over Iceland and positive (negative) values over the central North Atlantic  
574 Ocean. Association is also found between nodes 1, 2, 3, and 6 (5, 7, 8, and 9) and the positive (negative)  
575 phases of the AO index.

### 576 3.3 Downward radiative fluxes

577 Besides the anomalous circulation patterns, anomalous surface radiative fluxes may also play a role in  
578 shaping the spatial pattern of surface temperature variability. In fact, the spatial pattern of the mean  
579 anomalous daily downward longwave radiation for an individual node (Figure 4) is in good agreement  
580 with the spatial pattern of the surface temperature anomalies of that node. In other words, increased  
581 downward longwave radiation is associated with positive surface temperature anomalies, and vice  
582 versa. As expected from previous studies (e.g., Sedlar et al. 2011), there is a significant positive  
583 correlation between downward longwave radiative fluxes and the anomalous total column water vapor  
584 and mid-level cloud cover (not shown). The correlation to low- and high-level cloud cover is, however,  
585 not significant (~~Not~~ not shown). Most of the water vapor in both the Arctic and Eurasia is derived from  
586 the North Atlantic Ocean, but the water vapor is transported into the Arctic by southwesterly flows and  
587 into Eurasia by northwesterly winds. The anomalous shortwave radiation corresponding to each node  
588 (not shown) is an order of magnitude smaller than that of the longwave radiation anomalies and has a spatial

589 pattern opposite to that of the mid-level cloud cover and the longwave radiation anomalies.

#### 590 3.4 Sea ice

591 The analyses presented above attempt to explain the spatial pattern of surface temperature  
592 variability for each node from the perspective of anomalous heat advection and surface radiative fluxes.

593 As mentioned earlier, there has been a debate in the literature about the role played by the sea ice  
594 anomalies in the Barents and Kara Seas in the development of the warm Arctic-cold Eurasia pattern.

595 Here, we examine the anomalous turbulent heat flux (Figure 5) and sea ice concentration (Figure 6) for  
596 each node. Turbulent heat flux is considered positive when it is directed from the atmosphere  
597 downward to the ocean or land surfaces. Thus, a positive anomaly indicates either an increase in the  
598 atmosphere-to-surface heat transfer or a decrease in the heat transfer from the surface to the atmosphere.

599 The magnitude of anomalous turbulent heat flux is found to be comparable to that of anomalous  
600 downward longwave radiation (Figure 4). For all nodes, the heat flux anomalies are larger over ocean

601 than over land [\(Figure 5\)](#). For node 1, positive turbulent heat flux anomalies occur mainly over the

602 Barents Sea, the western and central North Atlantic Ocean and the eastern North Pacific Ocean,  
603 indicating an increase in heat transport from the air to the ocean due possibly to an increase in vertical

604 temperature gradient caused by warm air advection associated with anomalous circulation [\(Figures 2](#)  
605 [and 3\)](#). The downward heat transfer results in sea ice melt in the Greenland Sea and the Barents Sea

606 (Figure 6). For node 4, the anomalous southerly winds over the Nordic Sea produce larger positive

607 turbulent heat flux anomalies [\(Figure 5\)](#). For node 7, the anticyclone is located more northwards, which

608 generates opposite anomalous winds between the Nordic and northern Barents Seas and the southern

609 Barents Sea and thus opposite turbulent heat flux anomalies that are consistent with the opposite sea ice

610 concentration anomalies in the two regions [\(Figure 5\)](#). For nodes 3, 6, and 9, the anomalous cold air

611 from the central Arctic Ocean flows into warm water in the Nordic and Barents Seas, producing  
612 negative turbulent heat flux anomalies and positive sea ice concentration anomalies ([Figures 5 and 6](#)).  
613 Sorokina et al. (2016) noted that turbulent heat flux usually peaks 2 days before changes in surface  
614 temperature pattern occur. The pattern of the composited anomalous [500-hPa geopotential height](#),  
615 turbulent heat flux [and sea ice concentration](#) 2 days prior to the day when the nodes occur (not shown)  
616 is similar to the current-day pattern in [Figures 2, 65, and 6](#). Our results support the conclusion of  
617 Sorokina et al. (2016) and Blackport et al. (2019) that the anomalous atmospheric circulations lead to  
618 the anomalous sea ice concentration in the Barents Sea.

### 619 [3.5 Contributions of SOM nodes to the trends in wintertime surface temperature](#)

620 The results above suggest that both the surface temperature anomaly patterns over the Arctic Ocean  
621 and Eurasian continent and the sea ice concentration anomalies in the Nordic and Barents Seas can be  
622 explained largely by changes in atmospheric circulations and the associated vertical and horizontal heat  
623 and moisture transfer by mean and turbulent flows. Next, we assess the [trends of wintertime surface](#)  
624 [temperature and the](#) contributions of these [SOM](#) nodes to the [trends in wintertime surface temperature](#).

625 We first examine the time series of the accumulated number of days for each node in each winter  
626 for the 1979-2019 period (Figure 7). The time series for nodes 1, 4, 6, and 9 exhibit variability on  
627 interannual as well as decadal time scales. The occurrence frequency is noticeably larger after 2003  
628 than prior to 2003 for nodes 1 and 4, and vice versa for nodes 6 and 9, and the difference between the  
629 two periods is significant at 95% confidence level. Given the spatial patterns of these four nodes  
630 (Figure 1), this indicates that the warm Arctic-cold Eurasia pattern occurred more frequently after 2003.  
631 A linear trend analysis of the time series for each node (Table [23](#)) reveals significant positive trends in  
632 occurrence frequency for nodes 1 and 4 and significant negative trends for nodes 6 and 9, which agree

633 | with the result from a previous study (Clark and Lee, 2019; [Overland et al., 2015](#)) that suggested an  
634 | increasing trend of the warm Arctic and cold Eurasia pattern.

635 |       These trends in the occurrence frequency of the SOM nodes contribute to the trends in the total  
636 | wintertime (DJF) surface temperature anomalies (Figure 8, top panel) that have significant positive  
637 | trends over the Arctic Ocean and in regions of Northern and ~~Southern~~-Eastern Europe and negative,  
638 | [mostly insignificant](#) trends in Central Siberia. The contribution, however, varies from node to node  
639 | (Figure 9). Node 1 has the largest domain-averaged contribution of 18.7%, followed by its mirror node  
640 | (node 9) at 10.1%. Nodes 4 and 6 account for 2.8% and 4.3% of the total trend, respectively. None of  
641 | the remaining nodes explain more than 2%. All nodes together explain 39.5% of the total trend in  
642 | wintertime surface air temperature. The spatial pattern of the SOM-explained trends (Figure 8, middle  
643 | panel) is similar to the warm Arctic–cold continent pattern, whereas the residual trend resembles more  
644 | the total trend (Figure 8 bottom panel).

### 645 | 3.6 Mechanisms

646 |       The results presented above indicate that the SOM patterns explain nearly 40% of the trend in  
647 | wintertime surface air temperature anomalies and majority of the contributions (35 out of 40%) come  
648 | from the two pairs of the nodes (nodes 1, 9, and 4, 6). –The analyses hereafter will focus on these four  
649 | nodes. Below we assess the atmospheric and oceanic conditions associated with the occurrences of the  
650 | four nodes via regression analysis. Specifically, the anomalous seasonal SST and atmospheric  
651 | circulation variables are regressed onto the normalized time series of the number of days when each of  
652 | the four nodes occurs (Figures 10, 11, and 12).

653 |       For node 1, the SST regression pattern in the Pacific Ocean shows significant positive anomalies  
654 | over the tropical western Pacific Ocean and central North Pacific Ocean ([Figure 10](#)). The positive SST



655 anomalies also occur over most of the North Atlantic. Negative SST anomalies occur over the central  
656 tropical Pacific Ocean, though they are not significant at 95% confidence level. The SST regression  
657 pattern is reversed for node 9. The direction of wave activity flux indicates the direction of group speed  
658 of stationary planetary wave. Here we calculate the wave activity flux defined by Takaya and  
659 Nakamura (2001), which considers the influence of mid-latitude zonal wind (Figure 12). For node 1,  
660 ~~The~~ the corresponding anomalous 500-hPa height regression (Figure 11) shows two Rossby wavetrains:  
661 one is excited over the central Pacific Ocean and propagates northeastwards into North America and  
662 North Atlantic Ocean, and the other, which displays ~~a~~ the stronger signal, originates from central North  
663 Atlantic and propagates northeastwards to the Arctic Ocean and southeastwards to the Eurasian  
664 continent ~~and the western Pacific Ocean (Figure 11 and 12). The large SST anomalies over the Nordic~~  
665 ~~Ocean augment the wave signal through local air sea interaction. The wave activity flux and~~  
666 ~~streamfunction exhibit well the horizontal propagating direction of the planetary wave.~~ For node 9, the  
667 corresponding anomalous 500-hPa height and streamfunction show an opposite pattern, but the wave  
668 activity flux is similar to that of node 1.

669 For node 4, the SST anomalies over the tropical Pacific Ocean appear to be in a La Niña state,  
670 which shows stronger negative SST anomalies over the eastern tropical Pacific Ocean than those for  
671 node 1 (Figure 10). The positive SST anomalies over the North Pacific shift more northwards relative  
672 to that of node 1. The positive SST anomalies over the North Atlantic are weaker than those for node 1.  
673 The corresponding wavetrain over the Pacific Ocean is stronger than that over the Atlantic Ocean  
674 (Figure 11), which ~~is~~ seen also be observed in the pattern of wave activity and streamfunction (Figure  
675 12). The corresponding pattern for node 6 is nearly reversed, but there are some noticeable differences  
676 in the amplitude of the wavetrain and SST anomalies. For example, the magnitude of the anomalous

677 SST and the 500-hPa height over the central North Pacific is larger for node 6 than that for node 4.

678 Besides the above-mentioned variables, similar regression analysis is also performed for the  
679 anomalous 850-hPa wind field and anomalous downward longwave radiation (~~Not-not~~ shown). Their  
680 regression patterns, which are similar to those in Figures 3 and 4, explain well the decadal variability of  
681 the number of days for nodes 1, 4, 6, and 9. Together, these results [in Figures 10-12](#) indicate that the  
682 decadal variability of the occurrence frequency of the four nodes in recent decades is related to two  
683 wavetrains induced by SST anomalies over the central North Pacific Ocean and the North Atlantic  
684 Ocean ([Figures 10 and 11](#)). The aforementioned SST regression patterns over the Atlantic and Pacific  
685 Oceans also show features of the AMO and PDO (Figure 10). Since both the AMO and PDO exhibited  
686 a phase change in the late 1990s (Yu et al., 2017), the question is whether a similar change in the SOM  
687 frequency also appear in the late 1990s. A comparison of the averaged frequency before and after 1998  
688 shows a significant drop in frequency for nodes 6 and 9 and an increase in frequency for node 1 (~~not~~  
689 [shown](#)). This result suggests that the change in the AMO and PDO indices may contribute to the change  
690 in the frequencies of the warm Arctic-cold Eurasia continent pattern.

### 691 3.7 Interdecadal variability

692 The four-decade-long ERA-Interim reanalysis is not adequate for examining interdecadal to  
693 multi-decadal variations represented by the PDO and AMO indices. Further analysis is performed using  
694 the 20CR daily reanalysis data for the 1854-2014 period. Before applying the SOM technique to the  
695 20CR data, we first remove the trend to eliminate the influence from the global warming. No low-pass  
696 filter is applied before SOM analysis in order to test the stability of the SOM results for the different  
697 periods. The spatial SOM patterns from the de-trended century-long 20CR data (Figure 13) are similar  
698 to those for the 1979-2019 period (Figure 1). Nodes 1, 4, and 7 correspond to the positive phase of the

699 warm Arctic-cold Eurasia pattern and the negative phase can be observed in nodes 3, 6, and 9. The  
700 magnitude [in Figure 13](#) is smaller compared to the recent four decades [in Figure 1](#). The occurrence  
701 frequencies of ~~all~~ the [four nodes, 1, 4, 6, and 9](#) (Figure 14), are close to those for the recent four  
702 decades ([Figure 7](#)). It indicates that the SOM method can obtain stably the main modes of wintertime  
703 surface air temperature variability. For the recent four decades, the time series of the number of days  
704 also displays a noticeable increasing (decreasing) trend for nodes 1 and 4 (6 and 9), suggesting that the  
705 trend in the recent four decades is a reflection of an interdecadal variability of wintertime surface air  
706 temperature.

707 Next, we apply a 40-year low-pass filter to the time series of the occurrence frequencies for nodes  
708 1, 4, 6 and 9 and the AMO and PDO indices and calculate correlations. There is a significant  
709 correlation between the time series and the AMO index, with correlation coefficients of 0.36 for node 1,  
710 0.27 for node 4, -0.37 for node 6, and -0.20 for node 9, all of which are at the 95% confidence level. No  
711 significant correlations, however, are found between the filtered time series and the PDO index. If we  
712 define ~~a~~ SST index to represent the variability of SST anomalies over the central North Pacific Ocean  
713 (20°N-40°N, 150°E-150°W), the 40-year low-pass filtered central North Pacific Ocean SST index is  
714 now significantly correlated with the filtered time series of occurrence frequencies for nodes 1 and 9  
715 (0.55 for node 1 and -0.46 for node 9). The [correlation](#) results are consistent with the SST regression  
716 map for the recent decades (Figure 10).

717 To confirm the effect of SST anomalies on the warm Arctic -cold Eurasia pattern, we also perform  
718 EOF analysis of wintertime detrended seasonal surface air temperature anomalies for the 1854-2014  
719 period (Figure 15). The spatial patterns of the first and second EOF modes show the negative phase of  
720 the warm Arctic-cold Eurasia pattern and the 40-year low-pass filtered time series is inversely

721 correlated with the 40-year low-pass filtered wintertime AMO index (-0.46,  $p < 0.05$  for mode 1 and  
722 -0.44,  $p < 0.05$  for mode 2). The 40-year low-pass filtered time series of the two EOF modes have a  
723 significant negative correlation with the 40-year low-pass filtered central North Pacific Ocean SST  
724 index, with correlation coefficients of -0.19 and -0.26 ( $p < 0.05$ ). Only PC1 has a significant correlation  
725 with the PDO index (0.38,  $p < 0.05$ ). Thus, the increase in the occurrence of the warm Arctic-cold  
726 Eurasia pattern in the recent decades is a part of the interdecadal variability of the pattern, which is  
727 influenced by the AMO index, [the PDO index](#), and the central North Pacific SST.

#### 728 **4 Conclusions and Discussions**

729 In this study, we examine the variability of wintertime surface air temperature in the Arctic and the  
730 Eurasian continent (20°E-130°E) by applying the SOM method to daily temperature from the gridded  
731 ERA-Interim dataset for the period 1979-2019 and from the 20CR reanalysis for the period 1854-2014  
732 and the EOF method to seasonal temperature from the 20CR reanalysis for the period 1854-2014. The  
733 spatial pattern in the surface temperature variations in the study region, as revealed by the nine SOM  
734 nodes, is dominated by concurrent warming in the Arctic and cooling in Eurasia, and vice versa. The  
735 nine SOM patterns explain nearly 40% of the trends in wintertime surface temperature and 88% of that  
736 are accounted for by only four nodes. Two of the four nodes (nodes 1 and 4) represent the warm  
737 Arctic-cold Eurasian pattern and the other two (nodes 6 and 9) depict the opposite cold Arctic-warm  
738 Eurasia pattern. There is a clear shift in the frequency of the occurrence of these patterns near the  
739 beginning of this century, with the warm Arctic – cold Eurasia pattern dominating since 2003, while the  
740 opposite pattern prevailing from the 1980s through the 1990s. The warm Arctic-cold Eurasia pattern is  
741 accompanied by an anomalous high pressure and anticyclonic circulation over the Eurasian continent.  
742 The anomalous winds and the associated temperature and moisture advection interact with local

743 | longwave radiative forcing and turbulent [fluxes](#) to produce positive (negative) temperature anomalies  
744 | in the Arctic (Eurasian continent). The circulation is reversed for the cold Arctic-warm Eurasia pattern.  
745 | The warm, moist air mass advected to the Arctic by the anomalous atmospheric circulations and the  
746 | increased downward turbulent heat flux also explain sea ice melt in the Barents and Kara Seas. In other  
747 | words, the sea ice loss in the Barents and Kara Seas and the cooling of the Eurasian continent can both  
748 | be traced to anomalous atmospheric circulations.

749 |       Increasing occurrences of the warm Arctic-cold Eurasian continent pattern appear to relate to  
750 | rising SST over the central North Pacific and North Atlantic Oceans (positive AMO phase). The SST  
751 | anomalies trigger two Rossby wavetrains spanning from the North Pacific Ocean, North America, and  
752 | the North Atlantic Ocean to the Eurasian continent. The two wavetrains are strengthened through local  
753 | sea-atmosphere-ice interactions in mid-high latitudes, which influence the change in the occurrence  
754 | frequency of the warm Arctic-cold Eurasian continent pattern. Our results agree with those of previous  
755 | studies (Lee et al., 2011; Sato et al., 2014; Clark and Lee, 2019). But previous studies only focus on the  
756 | [effects](#) of SST anomalies over either North Pacific or North Atlantic Oceans. We also note that the two  
757 | wavetrains excited by SST anomalies over different oceans differ in amplitudes, leading to somewhat  
758 | different warm Arctic-cold Eurasia patterns.

759 |       Using century-long data, we show that the warm Arctic-cold Eurasia pattern is an intrinsic climate  
760 | mode, which has been stable since 1854. The recent increasing trend in its occurrence is a reflection of  
761 | an interdecadal variability of the pattern resulting from the interdecadal variability of SST anomalies  
762 | over the central Pacific Ocean and over the Atlantic Ocean represented by the AMO index. Sung et al.  
763 | (2018) investigated interdecadal variability of the warm Arctic and cold Eurasia pattern and considered  
764 | the variability of the SST over the North Atlantic as its origin. Our results suggest that the variability of

765 the SST over the North Pacific also plays an important role. However, internal atmospheric variability  
766 remains another potential source. The Rossby wavetrains also lead to deepening of a trough in East  
767 Asia and generate an anomalous low [pressure](#) and cold temperature in northern China ([Figure 10](#)),  
768 which further suggests that ~~the relationship between~~ a warmer Arctic, especially warmer Barents and  
769 Kara Seas ~~, and is not the driver for~~ the [increasing](#) occurrence of cold spells in East Asia, ~~as~~  
770 ~~suggested in~~ ~~may not be as strong as~~ ~~previously thought studies~~ (Kim et al., 2014; Mori et al., 2014;  
771 Kug et al., 2015; Overland et al., 2015).

772 ~~Our results suggest that the increasing trend in warm Arctic-cold Eurasia pattern may be related to~~  
773 ~~the anomalous SST over the central North Pacific and the North Atlantic Oceans. But we cannot rule~~  
774 ~~out the influence of the Arctic sea ice loss on the trend. Because the~~ ~~The Arctic sea ice loss results from~~  
775 ~~two main drivers: external and internal forcings. The former refers to the both Arctic warming due to~~  
776 ~~anthropogenic increasing of greenhouse gas concentrations and natural variability of ; the latter comes~~  
777 ~~from the climate system internal variability, such as anomalous SST anomalies. This study considers~~  
778 ~~natural variability or only the internal driver of climate system. The Arctic warming caused external~~  
779 ~~forcing related to increasing greenhouse gas emissions can produce an anomalous anticyclone over the~~  
780 ~~Barents and Kara Seas, leading to the warm Arctic-cold continents pattern.~~

781 ~~Although the ERA-Interim reanalysis is overall superior in describing~~ ~~has the best performance in~~  
782 ~~overall depiction of the Arctic atmospheric environment to other similar global reanalysis products, it~~  
783 ~~contains~~ ~~includes~~ ~~warm and moist biases in the surface layer~~ (Jakobson et al., 2012; Chaudhuri et al.,  
784 ~~2014; Simmons and Poli, 2015; Wang et al., 2019). However, we believe these biases, as well as the~~  
785 ~~relatively coarse resolution, should have minimum impact in the results from the current analyses.~~  
786 ~~Further, although the current analyses were performed on a predetermined SOM grid with 3x3 nodes,~~

787 [an increase in the number of SOM nodes didn't change the conclusions.](#)

788 Our results help broaden the current understanding of the formation mechanisms for the warm  
789 Arctic-cold Eurasia pattern. The SST anomalies over Northern Hemisphere oceans may offer a  
790 potential for predicting its occurrence. [The statistical relationship between SST anomalies and the](#)  
791 [occurrences of the warm Arctic-cold continents pattern may help improve the predictability of](#)  
792 [wintertime surface air temperature over Eurasian continent on interdecadal time scales.](#)

### 793 **Data Availability**

794 All data used in the current analyses are publicly available. The monthly sea ice concentration data are  
795 available from the National Snow and Ice Data Center (NSIDC) (<http://nsidc.org/data/NSIDC-0051>), the  
796 ERA-Interim reanalysis data are available from the European Center for Mid-Range Weather  
797 Forecasting (<https://www.ecmwf.int/en/forecasts/datasets/reanalysis-datasets/era-interim>) and the sea  
798 surface temperature data are available from the Hadley Centre for Climate Prediction and Research  
799 (<ftp://ftp.cdc.noaa.gov/Datasets/noaa.oisst.v2.highres/>). The long-term SST data are derived from  
800 from the Twentieth Century Reanalysis project, version 2c (20CR)  
801 (<https://climatedataguide.ucar.edu/climate-data/noaa-20th-century-reanalysis-version-2-and-2c>).

### 802 **Competing interests**

803 The authors declare that they have no conflict of interest.

### 804 **Author Contributions**

805 L. Yu designed the study, with input from S. Zhong, and carried out the analyses. L. Yu and S. Zhong  
806 prepared the manuscript. C. Sui plotted a part of Figures. [-B. Sun revised the manuscript.](#)

807 **Acknowledgements** We thank the European Centre for Medium-Range Weather Forecasts (ECMWF)  
808 for the ERA-Interim data. This study is financially supported by the National Key R&D Program of  
809 China (2019YFC1509102; 2017YFE0111700) and the National Natural Science Foundation of China  
810 (41922044).

811



812

813

814

815

816

817

818

819

820

821

822 **References**

823 Barnes, E. A. and Screen, J. A.: The impact of Arctic warming on the midlatitude jet-stream: Can it?

824 Has it? Will it?, WIREs Clim. Change, 6, 277-286, doi:10.1002/wcc.337, 2015.

825 Blackport, R., Screen J. A., Wiel K. van der, and Bintanja, R.: Minimal influence of reduced Arctic sea

826 ice on coincident cold winters in mid-latitudes, Nature Climate Change, 9,

827 doi:10.1038/s41558-019-0551-4, 2019, 2019.

828 [Chaudhuri, A. H., Ponte, R. M., and Nguyen, A. T.: A Comparison of atmospheric reanalysis products](#)

829 [for the Arctic Ocean and implications for uncertainties in air-sea fluxes, J. Climate, 27,](#)

830 [5411-5421, doi:10.1175/JCLI-D-13-00424.1, 2014.](#)

831 [Chen, L., Francis J. and Hanna E.: The “Warm-Arctic/Cold continents” pattern during 1901-2010.](#)

832 [Int. J. Climatol., 38, 5245-5254, ~~https://doi.org/doi:10.1002/joc.5725~~, 2018.](#)

833 Clark, J. P. and Lee, S.: The role of the tropically excited Arctic Warming Mechanism on the warm

834 Arctic cold continent surface air temperature trend pattern, *Geophys. Res. Lett.*, 46, 8490-8499,  
835 doi:10.1029/2019GL082714, 2019

836 Cohen, J., Screen, J. A., Furtado, J. C., Barlow, M., Whittleston, D., Coumou, D., Francis, J., Dethloff,  
837 K., Entekhabi, D., Overland, J., and Jones, J.: Recent Arctic amplification and extreme  
838 mid-latitude weather, *Nat. Geosci.*, 7, 627-637, doi:10.1038/ngeo2234, 2014.

839 Cohen, J., Pfeiffer, K., and Francis, J. A.: Warm Arctic episodes linked with increased frequency of  
840 extreme winter weather in the United States, *Nat. Commun.*, 9, 869,  
841 doi:10.1038/s41467-018-02992-9, 2018.

842 Compo, G. P., Whitaker, J. S., Sardeshmukh, P. D., Matsui, N., Allan, R., Yin, X., Jr, G. B. E., Vose, R.  
843 S., Rutledge, G. K., Bessemoulin, P., Brönnimann, S., Brunet, M., Crouthamel, R. I., Grant, A.  
844 N., Groisman, P. Y., Jones, P. D., Kruk, M. C., Kruger, A. C., Marshall, G. J., Maugeri, M., Mok,  
845 H. Y., Nordli, Ø., Ross, T. F., Trigo, R. M., Wang, X., Woodruff, S. D., and Worley S. J.: The  
846 Twentieth Century Reanalysis Project, *Quart. J. Roy. Meteor. Soc.*, 137, 1-28,  
847 doi:10.1002/qj.776, 2011.

848 Dee, D. P., Uppala, S. M., Simmons, A. J., Berrisford, P., Poli, P., Kobayashi, S., Andrac, U.,  
849 Balmaseda, M. A., Balsamo, G., Bauer, P., Bechtold, P., Beljaars, A. C. M., van de Berg, L.,  
850 Bidlot, J., Bormann, N., Delsol, C., Dragani, R., Fuentes, M., Geer, A. J., Haimberger, L., Healy,  
851 S. B., Hersbach, H., Hõm, E. V., Isaksen, L., Kålberg, P., Köhler, Matricardi, M., McNally, A.  
852 P., Monge-Sanz, B. M., Morcrette, J.-J., Park, B.-K., Peubey, C., de Rosnay, P., Tavolato, C.,  
853 Thépaut, J.-N., and Vitart, F.: The ERA-Interim reanalysis: configuration and performance of the  
854 data assimilation system. *Q. J. R. Meteorol. Soc.*, 137, 553-597, doi:10.1002/qj.828, 2011.

855 Enfield, D. B., Mestas-Nunez, A. M., and Trimble, P. J.: The Atlantic multidecadal oscillation and it's

856 relation to rainfall and river flows in the continental U.S., *Geophys. Res. Lett.*, 28, 2077-2080,  
857 2001.

858 Fyfe, J. C.: Midlatitudes unaffected by sea ice loss. *Nature Climate Change*, 9,  
859 doi:10.1038/s41558-019-0560-3, 2019 .

860 Gibson, P. B., Perkins-Kirkpatrick, S. E., Uotila, P., Pepler, A. S., and Alexander, L. V.: On the use of  
861 self-organizing maps for studying climate extremes, *J. Geophys. Res. Atmos.*, 122, 3891–3903,  
862 [doi:10.1002/2016JD026256](https://doi.org/10.1002/2016JD026256), 2017.

863 Hoskins, B. and Woollings, T.: Persistent extratropical regimes and climate extremes. *Curr. Clim. Change*  
864 *Rep.*, 1, 115-124, doi:10.1007/s40641-015-0020-8, 2015

865 Horton, D. E., Johnson, N. C., Singh, D., Swain, D. L., Rajaratnam, B., and Diffenbaugh, N. S.:  
866 Contribution of changes in atmospheric circulation patterns to extreme trends, *Nature*,  
867 522,465-469, doi:10.1038/nature14550, 2015.

868 Inoue, J., Hori, M. E., and Takaya, K.: The role of Barents Sea ice in the wintertime cyclone track and  
869 emergence of a warm-Arctic-Siberian anomaly, *J. Clim.*, 25, 2561-2568,  
870 doi:10.1175/JCLI-D-11-00449.1, 2012.

871 Jakobson, E., Vihma, T., Palo, T., Jakobson, L., Keernik, H., and Jaagus, J.: Validation of atmospheric  
872 reanalyses over the central Arctic Ocean, *Geophys. Res. Lett.*, 39, L10802,  
873 doi:10.1029/2012GL051591, 2012.

874 Johnson, N. C. and Feldstein, S. B.: The continuum of North Pacific sea level pressure patterns:  
875 Intraseasonal, interannual, and interdecadal variability, *J. Clim.*, 23,  
876 851-867, doi:10.1175/2009JCLI3099.1, 2010.

877 [Jakobson, E., Vihma, T., Palo, T., Jakobson, L., Keernik, H., Jaagus, J.: Validation of atmospheric](#)

878 | [reanalyses over the central Arctic Ocean, \*Geophys. Res. Lett.\*, 39, 2012.](#)

879 Kalnay, E., Kanamitsu, M., Kistler, R., Collins, W. G., Deaven, D., Gandin, L., Iredell, M., Saha, S.,  
880 White, G., Woollen J.: The NCEP/NCAR 40-year reanalysis project, *Bull. Amer. Meteor. Soc.*,  
881 77, 437-471, doi:10.1175/1520-0477(1996)077<0437:TNYRP>2.0.CO;2, 1996.

882 Kim, B.-M., Son, S.-W., Min, S.-K., Jeong, J.-H., Kim, S.-J., Zhang, X., Shim, T., and Yoon, J.-H.:  
883 Weakening of the stratospheric polar vortex by Arctic sea-ice loss, *Nature Commun.*, 5, 4646,  
884 doi:10.1038/ncomms5646, 2014.

885 Kohonen, T.: *Self-Organizing Maps*. 3<sup>rd</sup> ed. Springer, 501 pp, 2001.

886 Kug, J.-S., Jeong, J.-H., Jang, Y.-S., Kim, B.-M., Folland, C. K., Min, S.-K., and Son, S.-W.: Two  
887 distinct influences of Arctic warming on cold winters over North America and East Asia, *Nat.*  
888 *Geosci.*, 8, 759-762, doi:10.1038/ngeo2517, 2015.

889 Lee, S., Gong, T., Johnson, N., Feldstein, S. B., and Pollard, D.: On the possible link between tropical  
890 convection and the Northern Hemisphere Arctic surface air temperature change between 1958  
891 and 2001, *J. Clim.*, 24, 4350-4367, doi:10.1175/2011JCLI4003.1, 2011.

892 Lee, S. and Feldstein, S. B.: Detecting ozone- and greenhouse gas-driven wind trends with  
893 | observational data, *Science*, 339, 563-567, [doi:10.1126/science.1225154](#), 2013.

894 Loikith, P. C. and Broccoli, A. J.: Comparison between observed and model-simulated atmospheric  
895 circulation patterns associated with extreme temperature days over North America using CMIP5  
896 historical simulations, *J. Clim.*, 28, 2063-2079, doi:10.1175/JCLI-D-13-00544.1, 2015.

897 Luo, D., Xiao, Y., Yao, Y., Dai, A., Simmonds, I., and Franzke, C. L. E.: Impact of Ural blocking on  
898 winter warm Arctic-cold Eurasian anomalies. Part I: Blocking-induced amplification, *J. Clim.*,  
899 29, 3925-3947, doi:10.1175/JCLI-D-15-0611.1, 2016.

900 Mantua, N. J., Hare, S. R., Zhang, Y., Wallace, J. M., and Francis, R. C.: A Pacific interdecadal climate  
901 oscillation with impacts on salmon production, *Bull. Amer. Meteor. Soc.*, 78, 1069–1079, 1997.

902 Matsumura, S. and Kosaka, Y.: Arctic-Eurasian climate linkage induced by tropical ocean variability,  
903 *Nature Communications*, 10, 3441, doi:10.1038/s41467-019-11359-7, 2019.

904 Mori, M., Watanabe, M., Shiogama, H., Inoue, J., and Kimoto, M.: Robust Arctic sea-ice influence on  
905 the frequent Eurasian cold winters in past decades, *Nat. Geosci.*, 7, 869-873,  
906 doi:10.1038/ngeo2277, 2014.

907 Mori, M., Kosaka, Y., Watanabe, M., Nakamura, H., and Kimoto, M.: A reconciled estimate of the  
908 influence of Arctic sea-ice loss on recent Eurasian cooling, *Nat. Clim. Change*, 9, 123-129,  
909 doi:10.1038/s41558-018-0379-3, 2019.

910 McCusker, K. E., Fyfe, J. C., and Sigmond, M.: Twenty-five winters of unexcepted Eurasian cooling  
911 unlikely due to Arctic sea-ice loss, *Nat. Geosci.*, 9, 838-842, doi:10.1038/ngeo2820, 2016.

912 Overland, J. E., Wood, K. R., and Wang, M.: Warm Arctic-cold continents: climate impacts of the  
913 newly open Arctic sea, *Polar Res.*, 30, 15787, doi:10.3402/polar.v30i0.15787, 2011.

914 Overland, J. E., Francis, J., Hall, R., Hanna, E., Kim, S.-J., and Vihma, T.: The melting Arctic and  
915 Midlatitude weather patterns: Are they connected?, *J. Clim.*, 28, 7917-7932,  
916 doi:10.1175/JCLI-D-14-00822.1, 2015.

917 Palmer, T. N.: A nonlinear dynamical perspective on climate prediction, *J. Clim.*, 12, 575-591, 1999.  
918 doi:10.1175/1520-0442(1999)012<0575:ANDPOC>2.0.CO;2

919 Peings, Y.: Ural blocking as a driver of early-winter stratospheric warmings, *Geophys. Res. Lett.*, 46,  
920 5460-5468, doi:10.1029/2019GL082097, 2019.

921 Reusch, D. B., Alley, R. B., and Hewitson, B. C.: Relative performance of self-organizing maps and

922 principal component analysis in pattern extraction from synthetic climatological data, *Polar*  
923 *Geogr.*, 29, 188–212, doi:10.1080/789610199, 2005.

924 Reynolds, R. W., Smith, T. M., Liu, C., Chelton, D. B., Casey, K. S., Schlax, M. G.: Daily  
925 High-Resolution-Blended Analyses for Sea Surface Temperature, *J. Climate*, 20, 5473-5496,  
926 doi:10.1175/2007JCLI1824.1, 2007.

927 Sammon, J. W.: A non-linear mapping for data structure analysis. *IEEE Trans. Computers*, C-18,  
928 401–409 , 1969.

929 Sato, K., Inoue, J., and Watanabe, M.: Influence of the Gulf Stream on the Barents Sea ice retreat and  
930 Eurasian coldness during early winter, *Environ. Res. Lett.*, 9, 084009,  
931 doi:10.1088/1748-9326/9/8/084009, 2014.

932 Schudeboom, A., McDonald, A. J., Morgenstern, O., Harvey, M., and Parsons, S.: Regional  
933 regime-based evaluation of present-day GCM cloud simulations using self-organizing maps, *J.*  
934 *Geophys. Res. Atmos.*, 123, 4259–4272, doi:10.1002/2017JD028196, 2018.

935 Screen, J. A. and Simmonds, I.: The central role of diminishing sea ice in recent Arctic temperature  
936 amplification, *Nature*, 464, 1334-1337, doi:10.1038/nature09051, 2010.

937 Screen, J. S. and Simmonds, I.: Erroneous Arctic temperature trends in the ERA-40 reanalysis: A closer  
938 look, *J. Clim.*, 24, 2620–2627, doi:10.1175/2010JCLI4054.1, 2011.

939 Sedlar, J., Tjernström, M., Mauritsen, T., Shupe, M. D., Brooks, I. M., Persson, O., Birch, C. E., Leck,  
940 C., Sirevaag, A., and Nicolaus, M. : A transitioning Arctic surface energy budget: The impacts of  
941 solar zenith angle, surface albedo and cloud radiative forcing, *Clim. Dyn.*, 37, 1643–1660,  
942 [doi:10.1007/s00382-010-0937-5](https://doi.org/10.1007/s00382-010-0937-5), 2011.

943 Shepherd, T. G.: Effects of a warming Arctic, *Science*, 353, 989-990, doi:10.1126/science.aag2349,

944 2016.

945 [Simmons, A., and Poli, P.: Arctic warming in ERA-Interim and other analyses, Q. J. R. Meteorol. Soc.,](#)  
946 [141, 1147-1162, doi:10.1002/qj.2422, 2015.](#)

947 Skific, N., Francis, J. A., and Cassano, J. J.: Attribution of projected changes in atmospheric moisture  
948 transport in the Arctic: A self-organizing map perspective, J. Clim., 22, 4135-4153,  
949 doi:10.1175/2009JCLI2645.1, 2009.

950 Sorokina, S. A., Li, C., Wettstein, J. J., and Kvamstø, N. G.: Observed atmospheric coupling between  
951 Barents sea ice and the warm-Arctic cold-Siberian anomaly pattern, J. Clim., 29, 495-511,  
952 doi:10.1175/JCLI-D-15-0046.1, 2016.

953 Stroeve, J. C., Holland, M. M., Meier, W., Scambos, T., and Serreze, M.: Arctic sea ice decline: faster  
954 than forecast, Geophys. Res. Lett., 34, L09051, doi:10.1029/2007gl029703, 2007.

955 Stroeve, J. C.: Trends in Arctic sea ice extent from CMIP5, CMIP3 and observations, Geophys. Res.  
956 Lett., 39, L16502, doi:10.1029/2012GL052676, 2012.

957 Sun, L., Perlwitz, J., and Hoerling, M.: What caused the recent “warm Arctic-Cold Continents” trend  
958 pattern in winter temperature?, Geophys. Res. Lett., 43, 5345-5352,  
959 doi:10.1002/2016GL069024, 2016.

960 Sung, M.-K., Kim, S.-H., Kim, B.-M., and Choi, Y.-S.: Interdecadal variability of the warm Arctic and  
961 cold Eurasia pattern and its North Atlantic origin, Journal of Climate, 31, 5793-5810,  
962 doi:10.1175/JCLI-D-17-0562.1, 2018.

963 Tang, Q., Zhang, X., Yang, X., and Francis J. A.: Cold winter extremes in northern conditions linked to  
964 Arctic sea ice loss, Environ. Res. Lett., 8, 014036, doi:10.1088/1748-9326/8/1/014036, 2013.

965 Takaya K, and Nakamura, H.: A formulation of a phase-independent wave-activity flux for stationary

966 and migratory quasigeostrophic eddies on a zonally varying basic flow, *J. Atmos. Sci.*, 58,  
967 608-627, 2001.

968 Uppala, S., KÅllberg, P. W., Simmons, A. J., Andrae, U., Da Costa Bechtold, V., Florino, M., Gibson, J.  
969 K., Haseler, J., Hernandez, A., Kelly, G. A., Li, X., Onogi, K., Saarinen, S., Sokka, N., Allan, R.  
970 P., Andersson, E., Arpe, K., Balmaseda, M. A., Beljaars, A. C. M., Van De Berg, L., Bidlot, J.,  
971 Bormann, N., Caires, S., Chevallier, F., Dethof, A., Dragosavac, M., Fisher, M., Fuentes, M.,  
972 Hagemann, S., Hm, E., Hoskins, B. J., Isaksen, L., Janssen, P. A. E. M., Jenne, R., McNally, A.  
973 P., Mahfouf, J.-F., Morcrette, J.-J., Rayner, N. A., Saunders, R. W., Simon, P., Sterl, A.,  
974 Trenberth, K. E., Untch, A., Vasiljevic, D., Viterbo, P., and Woollen, J.: The ERA-40 re-analysis,  
975 *Quarterly Journal of the Royal Meteorological Society*, 131, 2961–3012, doi:10.1256/qj.04.176,  
976 2005.

977 Walsh, J. E.: Intensified warming of the Arctic: Causes and impacts on middle Latitudes, *Glob. Planet.*  
978 *Change*, 117, 52-63, doi:10.1016/j.gloplacha.2014.03.003 , 2014.

979 Vihma, T.: Effects of Arctic sea ice decline on weather and climate: A review, *Surv. Geophys.*, 35,  
980 1175-1214, doi:10.1007/s10712-014-9284-0 , 2014.

981 Vihma, T., Graverson, R., Chen, L., Handorf, D., Skific, N., Francis, J. A., Tyrrell, N., Hall, R., Hanna,  
982 E., Uotila, P., Dethloff, K., Karpechko, A. Y., Björnsson, H., and Overland, J. E.: Effects of the  
983 tropospheric large-scale circulation on European winter temperatures during the period of amplified  
984 Arctic warming, *Int. J. Climatol.*, doi:10.1002/joc.6225, 2019.

985 [Wang, C., Graham, R. M., Wang, K., Gerland, S., Granskog, M. A.: Comparison of ERA5 and](#)  
986 [ERA-Interim near-surface air temperature, snowfall and precipitation over Arctic sea ice: effects](#)  
987 [on sea ice thermodynamics and evolution, \*The Cryosphere\*, 13, 1661-1679, 2019.](#)



988 Yoo, C., Feldstein, S., and Lee, S.: The impact of the Madden–Julian oscillation trend on the Arctic  
989 amplification of surface air temperature during the 1979–2008 boreal winter, *Geophys. Res.*  
990 *Lett.*, 38, L24804, doi:10.1029/2011GL049881, 2011.

991 Yu, L., Zhong, S., Winkler, J. A., Zhou, M., Lenschow, D. H., Li, B., Wang, X., and Yang, Q.: Possible  
992 connections of the opposite trends in Arctic and Antarctic sea-ice cover, *Scientific Reports*, 7,  
993 45804, doi:10.1038/srep45804, 2017.

994

995

996

997 Table 1. Spatial correlations (Corrs) between the daily winter (DJF) surface air  
 998 temperature and the corresponding SOM pattern for each day from 1979 to 2018.

	3×1	2×2	3×2	4×2	3×3	5×2	4×3	5×3	4×4
Corr	0.26	0.43	0.48	0.48	0.50	0.49	0.50	0.51	0.51

999

1000

1001

1002

1003

1004

1005

1006

1007

1008

1009

1010

1011

1012

1013

1014

1015

1016

1017

1018

1019

1020

1021

1022

1023

1024

1025

1026

1027

1028

1029 Table 2. Averaged anomalous NAO and AO indices for all occurrences of each SOM  
 1030 node. Asterisks indicate the above 95% confidence level.

1031

	Node1	Node2	Node3	Node4	Node5	Node6	Node7	Node8	Node9
NAO	0.38*	0.22*	0.12*	0.05	-0.22*	-0.02	-0.07	-0.31*	-0.32*
AO	0.44*	0.38*	1.03*	-0.42	-0.62*	0.22*	-0.44*	-1.11*	-0.41*

1032

1033

1034

1035

1036

1037

1038

1039

1040

1041

1042

1043

1044

1045

1046

1047

1048

1049

1050

1051

1052

1053

1054

1055

1056

1057

1058

1059

1060

1061

1062

1063

1064

1065

1066

1067

1068

1069

1070 Table 3. Trends in the frequency of occurrences for each SOM node (day yr<sup>-1</sup>).  
 1071 Asterisks indicate the above 95% confidence level.  
 1072

	Node1	Node2	Node3	Node4	Node5	Node6	Node7	Node8	Node9
Trend	0.80*	0.10	-0.18	0.22*	-0.02	-0.39*	0.17	-0.17	-0.50*

1073  
 1074  
 1075  
 1076  
 1077  
 1078  
 1079  
 1080  
 1081  
 1082  
 1083  
 1084  
 1085  
 1086  
 1087  
 1088  
 1089  
 1090  
 1091  
 1092  
 1093  
 1094  
 1095  
 1096  
 1097  
 1098  
 1099  
 1100  
 1101  
 1102  
 1103  
 1104  
 1105  
 1106  
 1107  
 1108  
 1109

1110 Table 4. Frequencies of occurrence (%) of wintertime surface air temperature patterns  
 1111 in Figure 1 for all winters before 1998 and after 1998 for the period 1979-2019.  
 1112 Values with Asterisks are significantly different from climatology above the 95%  
 1113 confidence level.  
 1114

SOM patterns	Frequencies of occurrence		
	All winters	Winters before 1998	Winters after 1998
Node 1	17.1	7.4*	26.8
Node 2	4.4	3.3	5.4
Node 3	17.2	18.8	15.6
Node 4	8.6	5.4	11.7
Node 5	3.4	3.4	3.5
Node 6	10.2	15.2*	2.1*
Node 7	13.7	10.6	16.8
Node 8	10.1	12.1	8.0
Node 9	15.4	23.7*	7.1*

1115  
 1116  
 1117  
 1118  
 1119  
 1120  
 1121  
 1122  
 1123  
 1124  
 1125  
 1126  
 1127  
 1128  
 1129  
 1130  
 1131  
 1132  
 1133  
 1134  
 1135  
 1136  
 1137  
 1138  
 1139  
 1140  
 1141

1142 **Figure Captions**

1143 Figure 1. Spatial patterns of SOM nodes for daily wintertime (December, January, and  
1144 February) surface air temperature anomalies ( °C) without removing their linear trends  
1145 from ERA-Interim reanalysis over the 1979-2019 period. The number in brackets  
1146 denotes the frequency of the occurrence for each node.

1147 Figure 2. Corresponding 500-hPa geopotential height anomalies (gpm) without  
1148 removing their linear trends from ERA-Interim reanalysis over the 1979-2019 period  
1149 for each node in Figure 1. Dotted regions indicate the above 95% confidence level.  
1150 The thick black lines show the study region.

1151 Figure 3. Corresponding anomalous 850-hPa wind field ( $\text{ms}^{-1}$ ) without removing ~~the~~  
1152 its linear trend from ERA-Interim reanalysis over the 1979-2019 period for each node  
1153 in Figure 1. Shaded regions indicate the above 95% confidence level. The thick black  
1154 lines show the study region.

1155 Figure 4. Corresponding anomalous daily accumulated downward longwave radiation  
1156 ( $105 \text{ W m}^{-2}$ ) without removing ~~the~~ its linear trend from ERA-Interim reanalysis over  
1157 the 1979-2019 period for each node in Figure 1. Dotted regions indicate the above 95%  
1158 confidence level. The thick black lines denote show the study region.

1159 Figure 5. Corresponding anomalous daily accumulated turbulent heat flux (sensible  
1160 and latent heat) ( $10^5 \text{ W m}^{-2}$ ) without removing their linear trends from ERA-Interim  
1161 reanalysis over the 1979-2019 period for each node in Figure 1. Positive values  
1162 denote heat flux from atmosphere to ocean and vice versa. Dotted regions indicate the  
1163 above 95% confidence level. The thick black lines denote show the study region.

1164 Figure 6. Corresponding anomalous wintertime sea ice concentration without  
1165 removing ~~the-its linear~~ trend from the NSIDC over the 1979-2019 period for each  
1166 node in Figure 1. Dotted regions indicate the above 95% confidence level.

1167 Figure 7. Time series of the number of days for occurrence of each SOM node in  
1168 Figure 1 over the 1979-2019 period. The thick lines denote the trend in time series.

1169 Figure 8. Total (top), SOM-explained (middle), and residual (bottom) trend in  
1170 wintertime (DJF) surface air temperature ( $^{\circ}\text{C yr}^{-1}$ ) over the 1979-2019 period. Dots in  
1171 the top panel indicate above 95% confidence level.

1172 Figure 9. Trends in surface air temperature explained by each SOM node ( $^{\circ}\text{C yr}^{-1}$ )  
1173 over the 1979-2019 period. The percentage in the upper of each panel indicates the  
1174 fraction of the total trend represented by each node.

1175 Figure 10. Anomalous SST ( $^{\circ}\text{C}$ ) regressed into the normalized time series of  
1176 occurrence number for nodes 1, 4, 6, and 9 without removing ~~the-its linear~~ trend from  
1177 the NOAA over the 1979-2019 period.

1178 Figure 11. Anomalous 500-hPa geopotential height (gpm) regressed into the  
1179 normalized time series of occurrence number for nodes 1, 4, 6, and 9 without  
1180 removing ~~the-its linear~~ trend from ERA-Interim reanalysis over the 1979-2019 period.

1181 Figure 12. The anomalous wave activity flux (vectors) (Takaya and Nakamura, 2001)  
1182 and stream function (colors, units:  $10^7 \text{ m}^2 \text{ s}^{-1}$ ) regressed onto the normalized time  
1183 series of occurrence number for nodes 1, 4, 6, and 9 without removing ~~the-their linear~~  
1184 trends from ERA-Interim reanalysis over the 1979-2019 period.

1185 Figure 13. Spatial patterns of SOM nodes for detrended daily wintertime (December,

1186 January, and February) surface air temperature anomalies ( $^{\circ}\text{C}$ ) from the 20CR  
1187 reanalysis for the 1851-2014 period. The number in brackets denotes the frequency of  
1188 the occurrence for each node.

1189 Figure 14. Time series of the number of days for occurrence of each SOM node in  
1190 Figure 13 from the 20CR reanalysis for the 1851-2014 period. The thick red lines  
1191 denote the result in Figure 7 from the ERA-Interim reanalysis for the 1979-2019  
1192 period.

1193 Figure 15. The (a) leading pattern and (b) its time series (PC1 and PC2) of EOF  
1194 analysis of wintertime surface air temperature anomalies from the 20CR reanalysis for  
1195 the 1851-2014 period. Prior to EOF analysis, surface air temperature data are  
1196 detrended. A 40-yr low-pass filter is applied to the time series of PC1, PC2, AMO,  
1197 PDO, and central North Pacific Ocean (CNPO) indices. The correlation coefficients  
1198 between PC1 and AMO, PDO and CNPO indices are -0.46 ( $p < 0.0001$ ), 0.38  
1199 ( $p < 0.0001$ ), and -0.19 ( $p = 0.019$ ); those between PC2 and AMO, PDO and CNPO  
1200 indices are -0.44 ( $p < 0.0001$ ), 0.38 ( $p < 0.0001$ ), and -0.26 ( $p = 0.0009$ ).

1201

1202

1203

1204

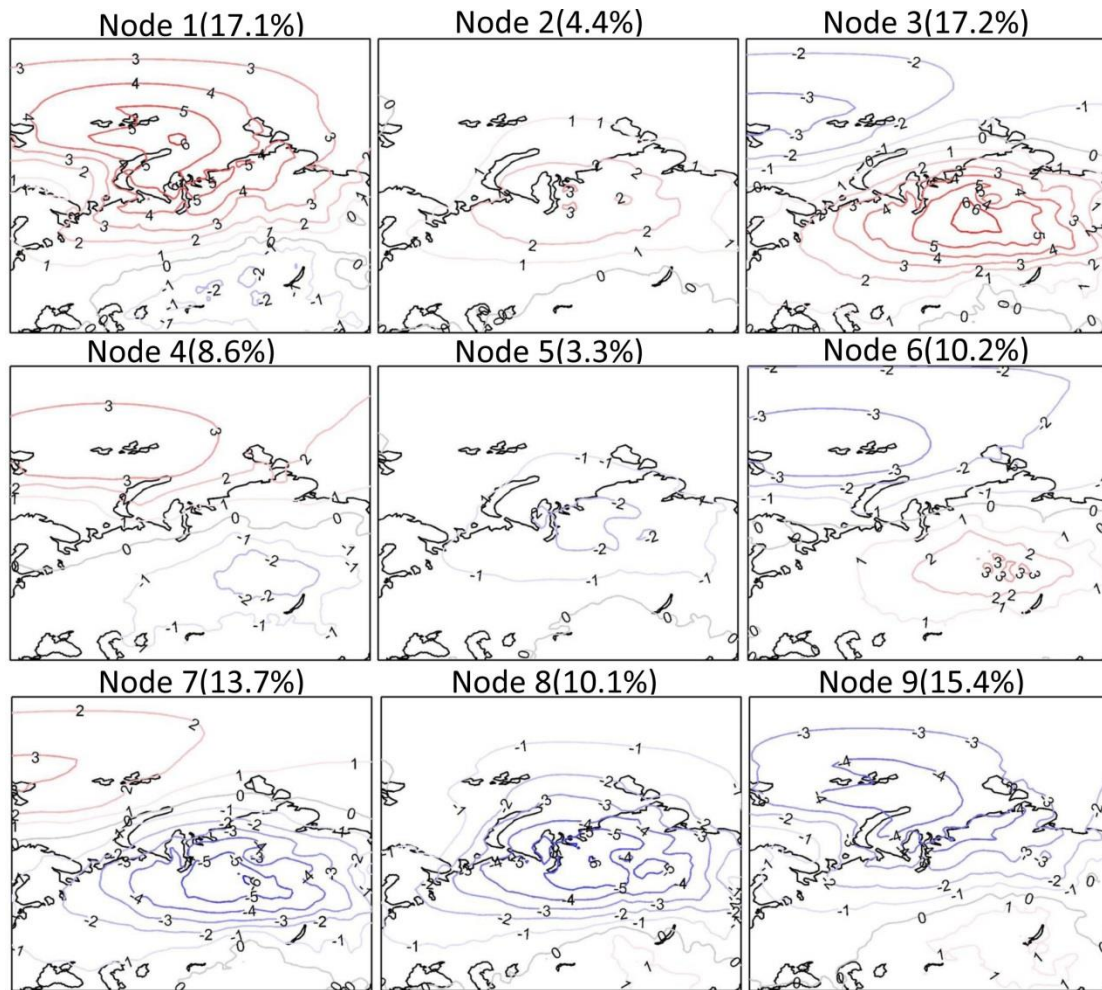
1205

1206

1207



1208



1209

1210

1211

1212

1213

1214

1215

1216

1217

1218

1219

1220

1221

1222

1223

1224

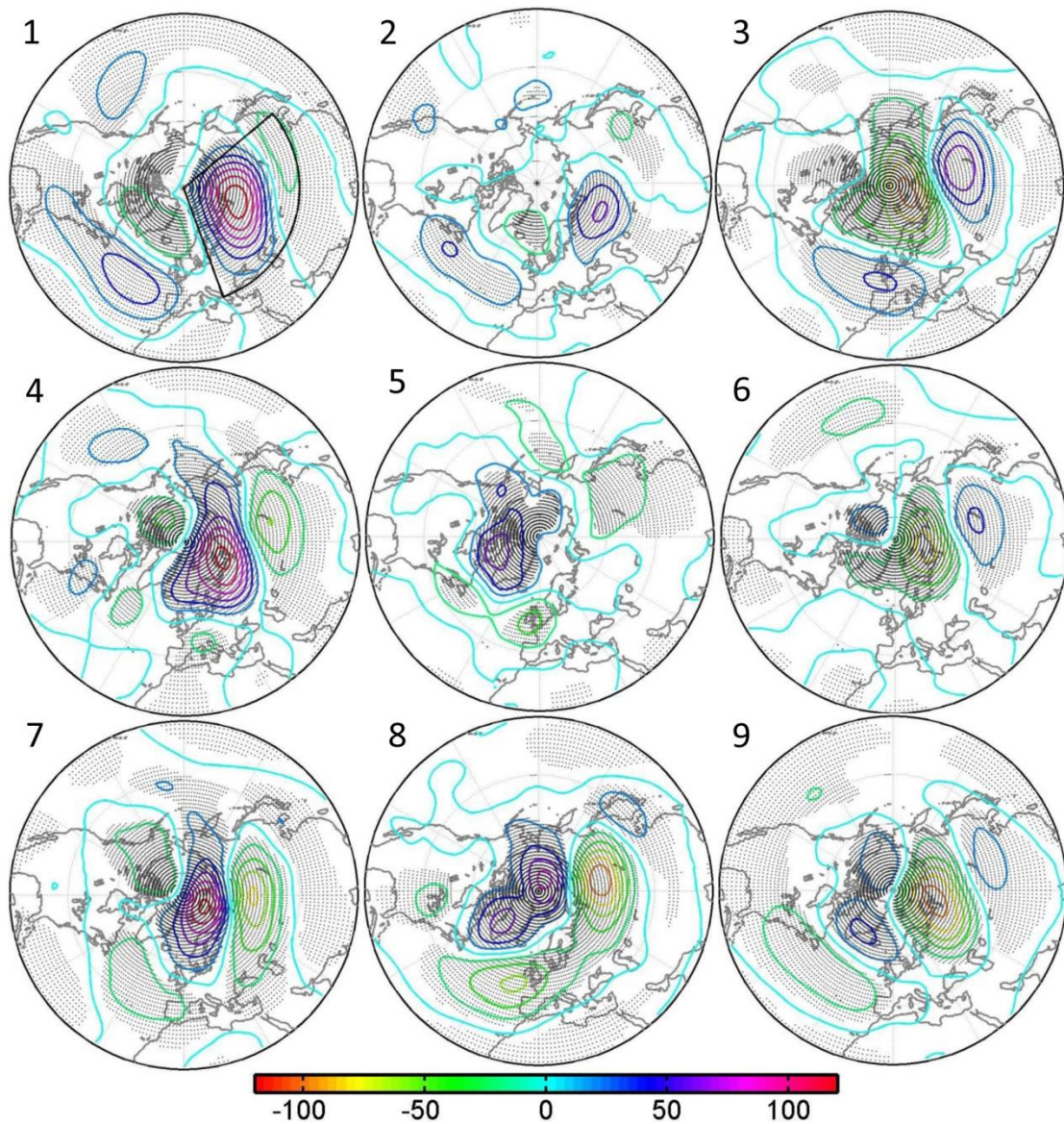
1225

1226

1227

1228

Figure 1. Spatial patterns of SOM nodes for daily wintertime (December, January, and February) surface air temperature anomalies ( $^{\circ}\text{C}$ ) without removing their linear trends from ERA-Interim reanalysis over the 1979-2019 period. The number in brackets denotes the frequency of the occurrence for each node.

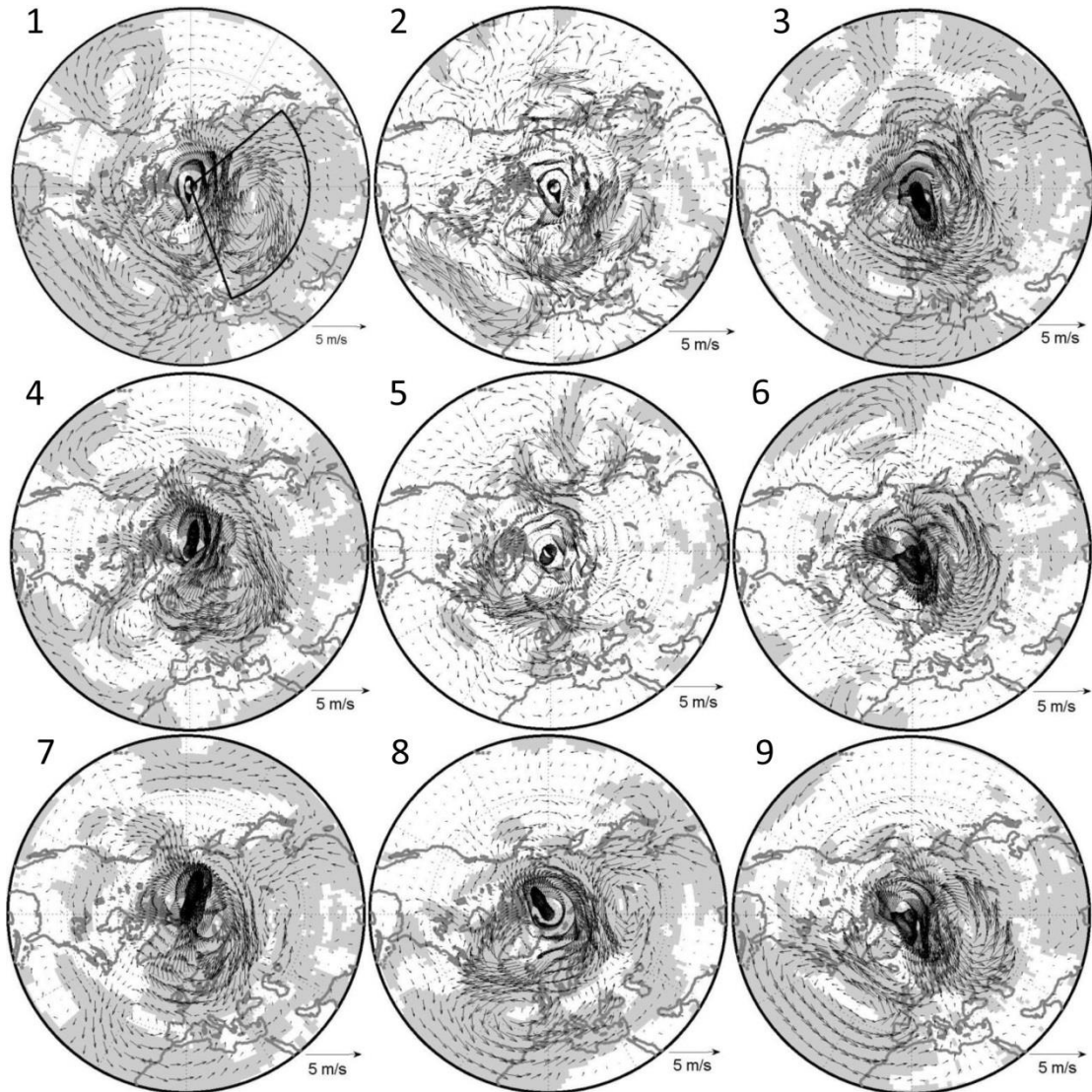


1230  
 1231  
 1232  
 1233  
 1234  
 1235  
 1236  
 1237  
 1238  
 1239  
 1240  
 1241  
 1242  
 1243  
 1244  
 1245

Figure 2. Corresponding 500-hPa geopotential height anomalies (gpm) without removing their linear trends from ERA-Interim reanalysis over the 1979-2019 period for each node in Figure 1. Dotted regions indicate the above 95% confidence level. The thick black lines denote-show the study region.



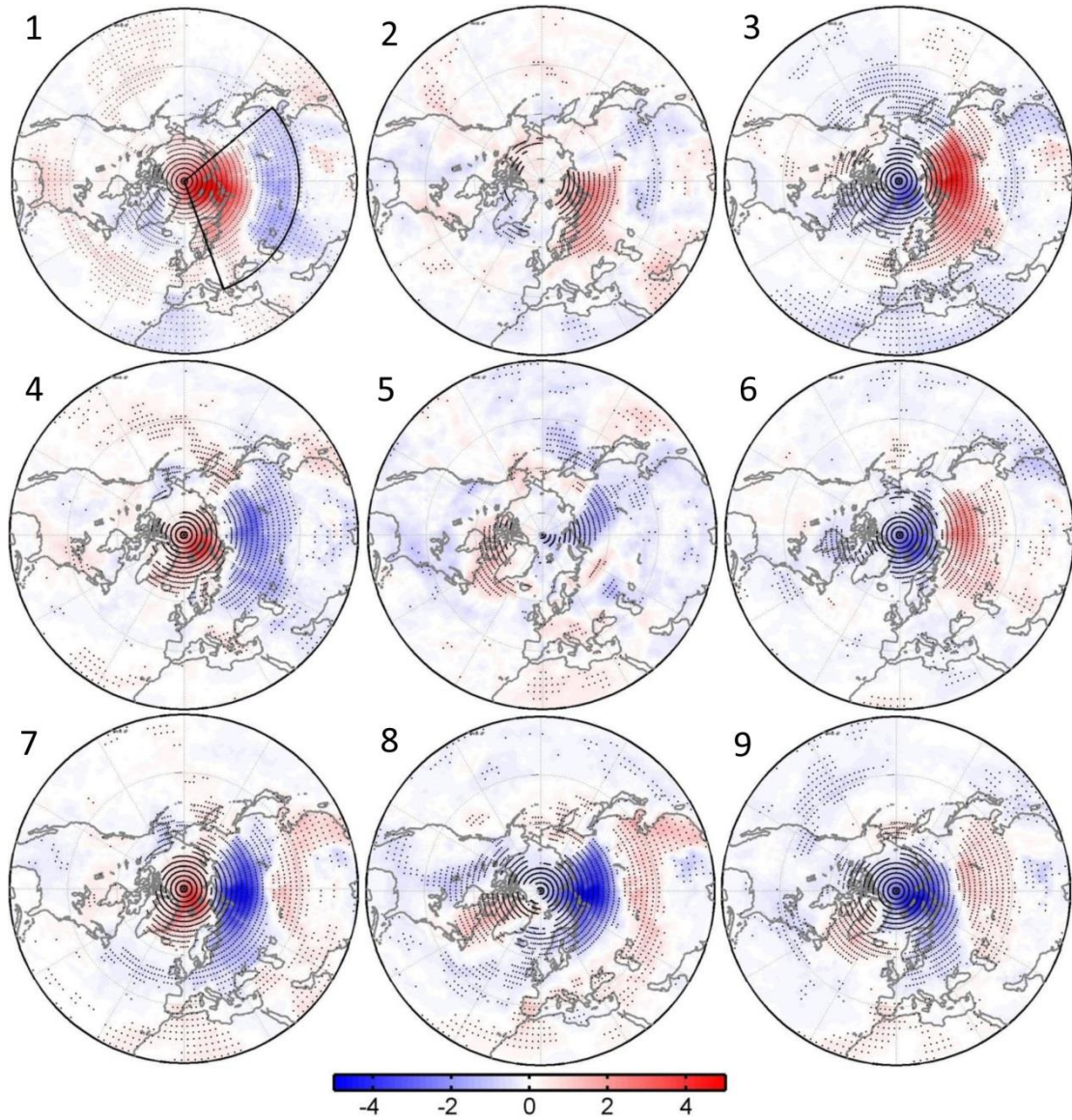
1246  
1247  
1248



1249  
1250  
1251  
1252  
1253  
1254  
1255  
1256  
1257  
1258  
1259  
1260  
1261  
1262  
1263

Figure 3. Corresponding anomalous 850-hPa wind field ~~( $\text{ms}^{-1}$ )~~ without removing its linear trend from ERA-Interim reanalysis over the 1979-2019 period for each node in Figure 1. Shaded regions indicate the above 95% confidence level. The thick black lines ~~denotes~~ show the study region.

1264  
1265  
1266  
1267  
1268  
1269

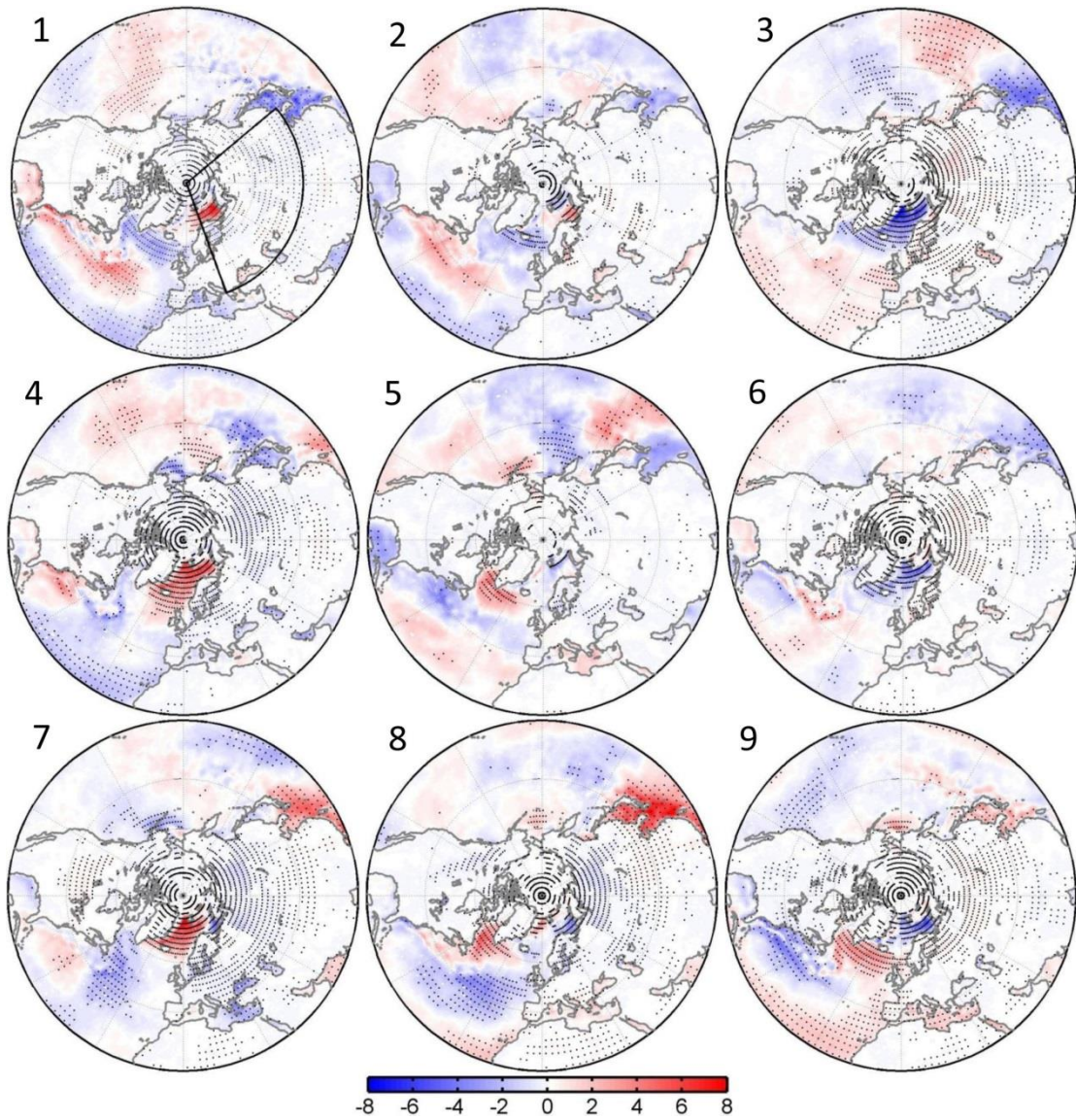


1270  
1271  
1272  
1273  
1274  
1275  
1276  
1277  
1278  
1279  
1280

Figure 4. Corresponding anomalous daily accumulated downward longwave radiation ( $10^5 \text{ W m}^{-2}$ ) without removing its linear trend from ERA-Interim reanalysis over the 1979-2019 period for each node in Figure 1. Dotted regions indicate the above 95% confidence level. The thick black lines denote-show the study region.



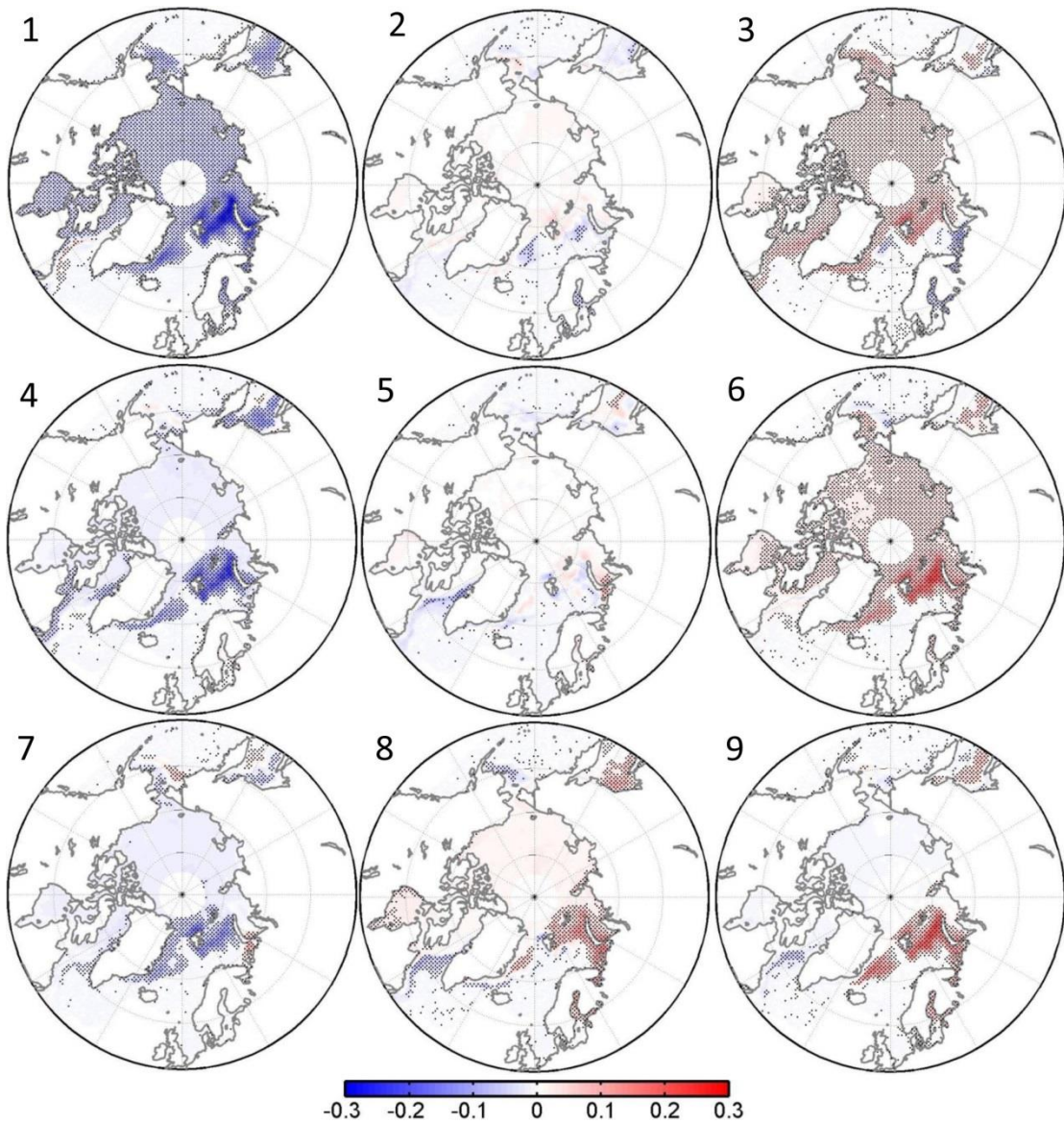
1281  
1282  
1283  
1284  
1285  
1286  
1287  
1288  
1289



1290  
1291  
1292  
1293  
1294  
1295  
1296  
1297

Figure 5. Corresponding anomalous daily accumulated turbulent heat flux (sensible and latent heat) ( $10^5 \text{W m}^{-2}$ ) without removing their linear trends from ERA-Interim reanalysis over the 1979-2019 period for each node in Figure 1. Positive values denote heat flux from atmosphere to ocean and vice versa. Dotted regions indicate the above 95% confidence level. The thick black lines denote show the study region.

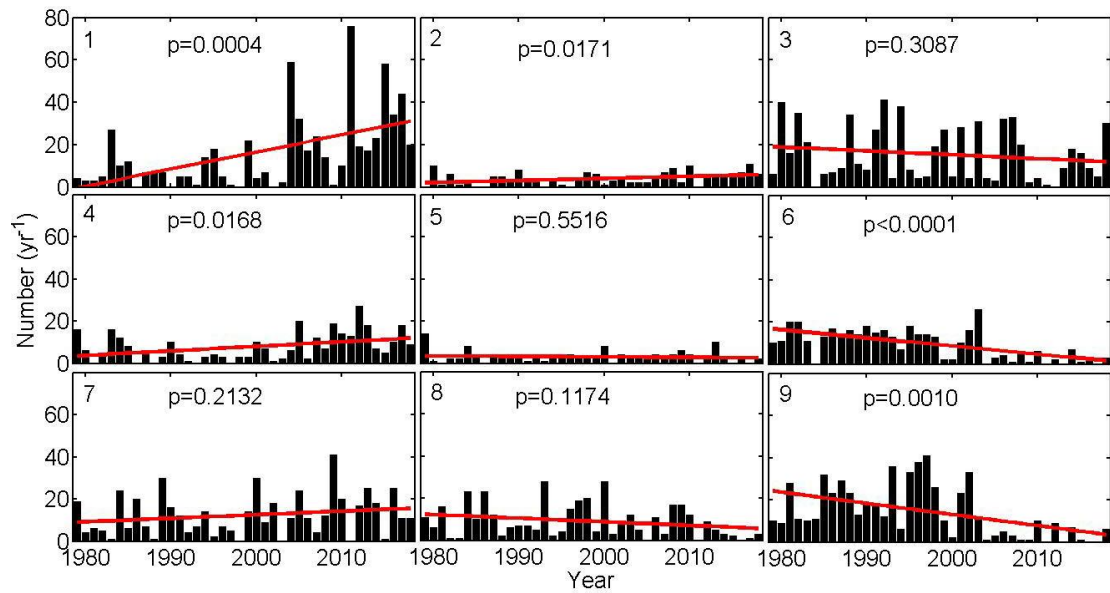
1298  
1299  
1300  
1301  
1302  
1303  
1304  
1305  
1306  
1307  
1308  
1309



1310  
1311  
1312  
1313  
1314

Figure 6. Corresponding anomalous wintertime sea ice concentration without removing its linear trend from the NSIDC over the 1979-2019 period for each node in Figure 1. Dotted regions indicate the above 95% confidence level.

1315  
1316  
1317  
1318  
1319  
1320  
1321  
1322  
1323  
1324  
1325  
1326  
1327  
1328  
1329

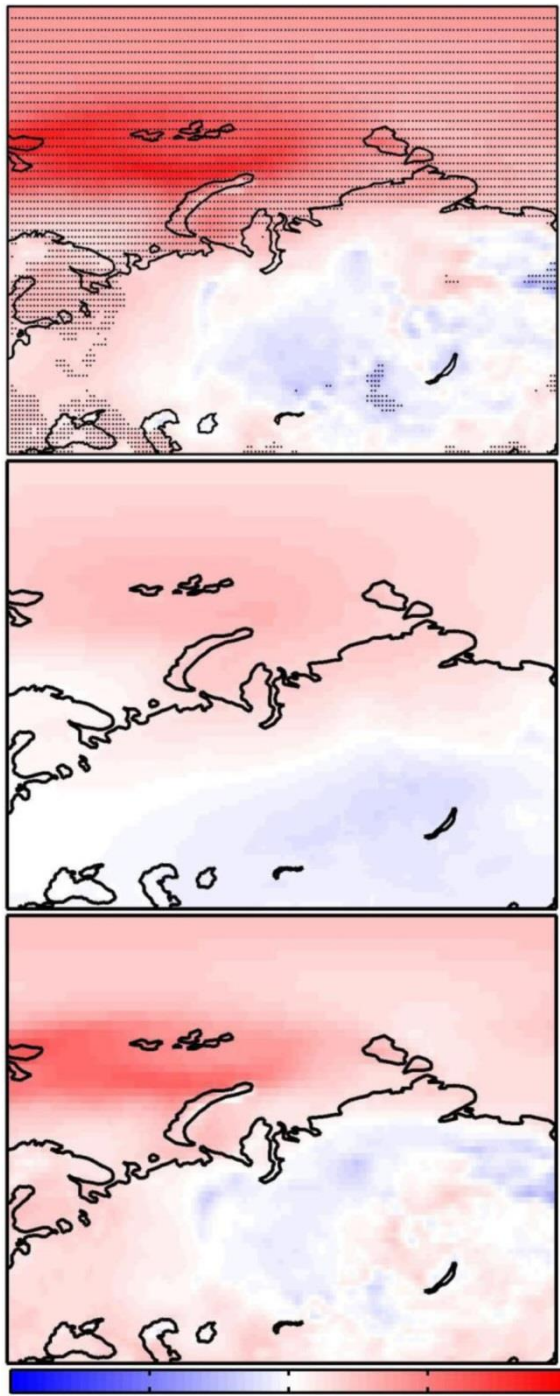


1330  
1331  
1332  
1333  
1334  
1335  
1336  
1337  
1338  
1339  
1340  
1341  
1342  
1343  
1344

Figure 7. Time series of the number of days for occurrence of each SOM node in Figure 1 over the 1979-2019 period. The thick lines denote the trend in time series.

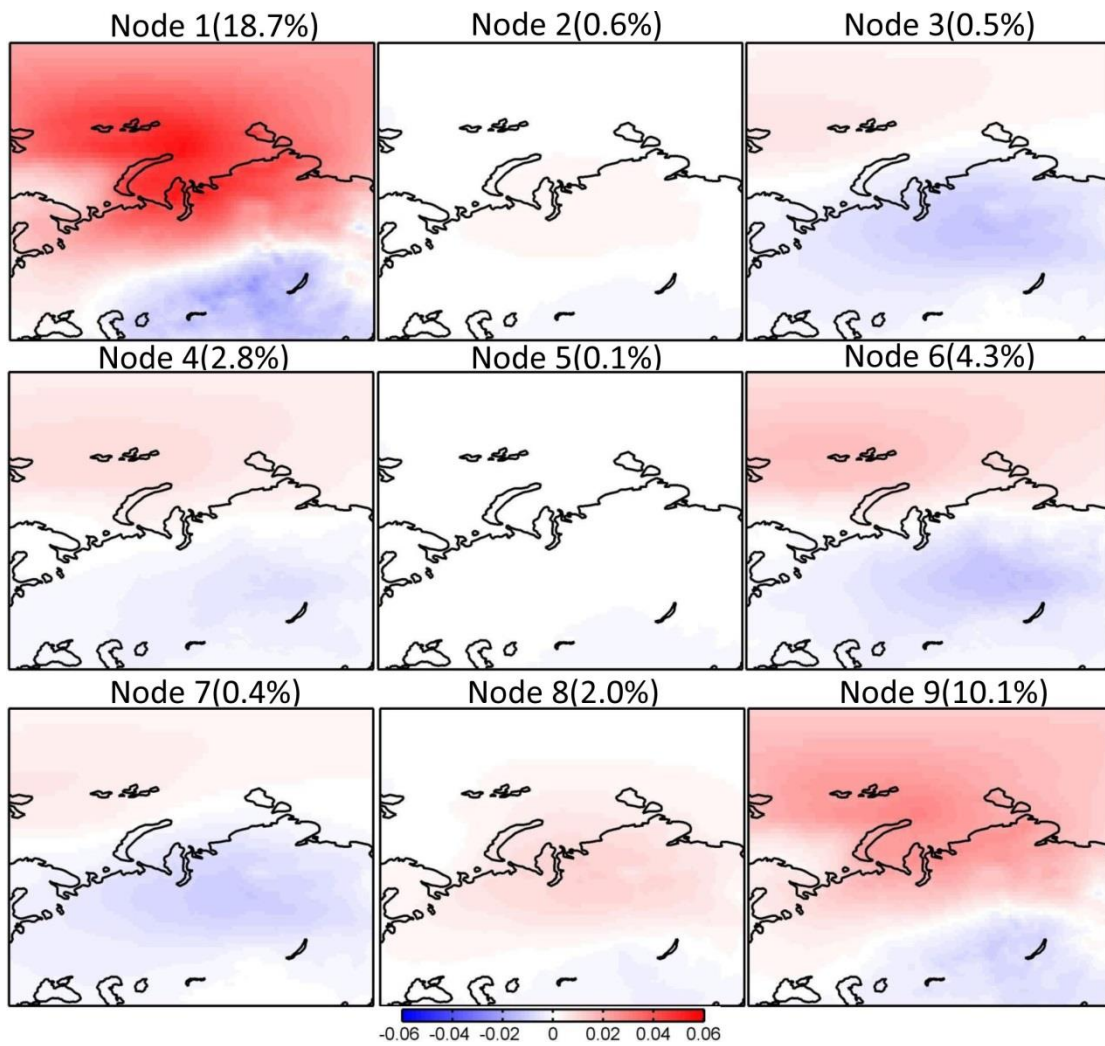


1345  
1346  
1347



1348 -0.4 -0.2 0 0.2 0.4  
1349 Figure 8. Total (top), SOM-explained (middle), and residual (bottom) trend in wintertime (DJF)  
1350 surface air temperature ( $^{\circ}\text{C yr}^{-1}$ ) over the 1979-2019 period. Dots in the top panel indicate above  
1351 95% confidence level.  
1352

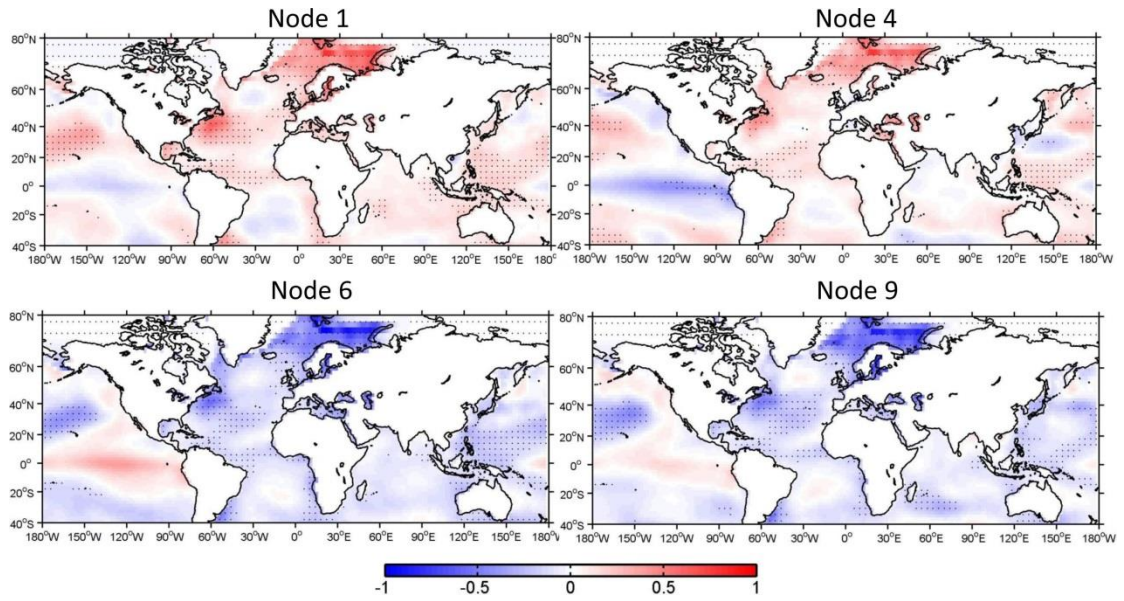




1353  
1354  
1355  
1356  
1357  
1358  
1359  
1360  
1361  
1362  
1363  
1364  
1365  
1366  
1367  
1368  
1369  
1370  
1371  
1372

Figure 9. Trends in surface air temperature explained by each SOM node ( $^{\circ}\text{C yr}^{-1}$ ) over the 1979-2019 period. The percentage in the upper of each panel indicates the fraction of the total trend represented by each node.

1373  
1374



1375

1376 Figure 10. Anomalous SST ( $^{\circ}\text{C}$ ) regressed into the normalized time series of occurrence number  
1377 for nodes 1, 4, 6, and 9 without removing its linear trend from the NOAA over the 1979-2019  
1378 period.

1379

1380

1381

1382

1383

1384

1385

1386

1387

1388

1389

1390

1391

1392

1393

1394

1395

1396

1397

1398

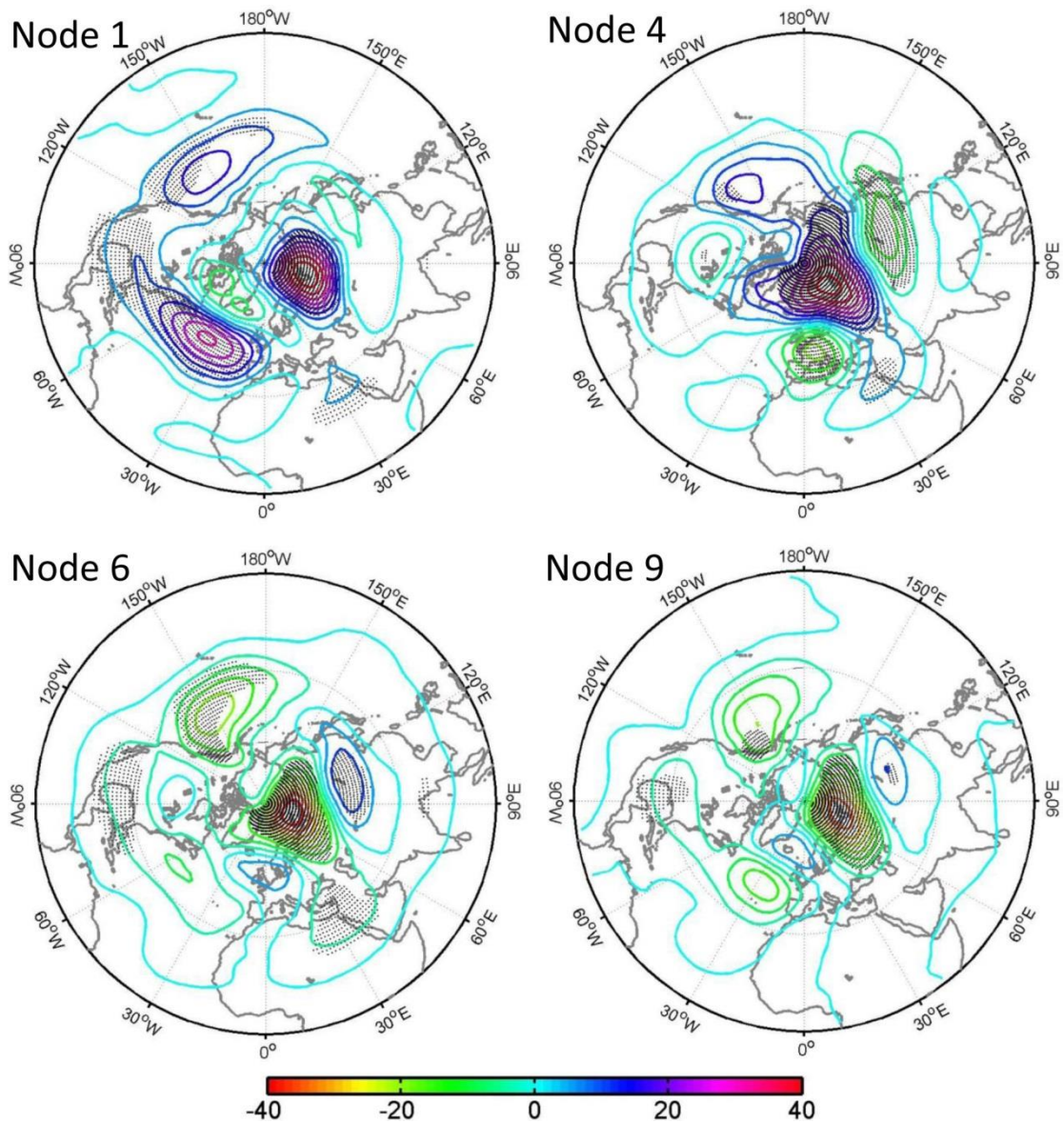
1399

1400

1401

1402

1403  
1404  
1405  
1406

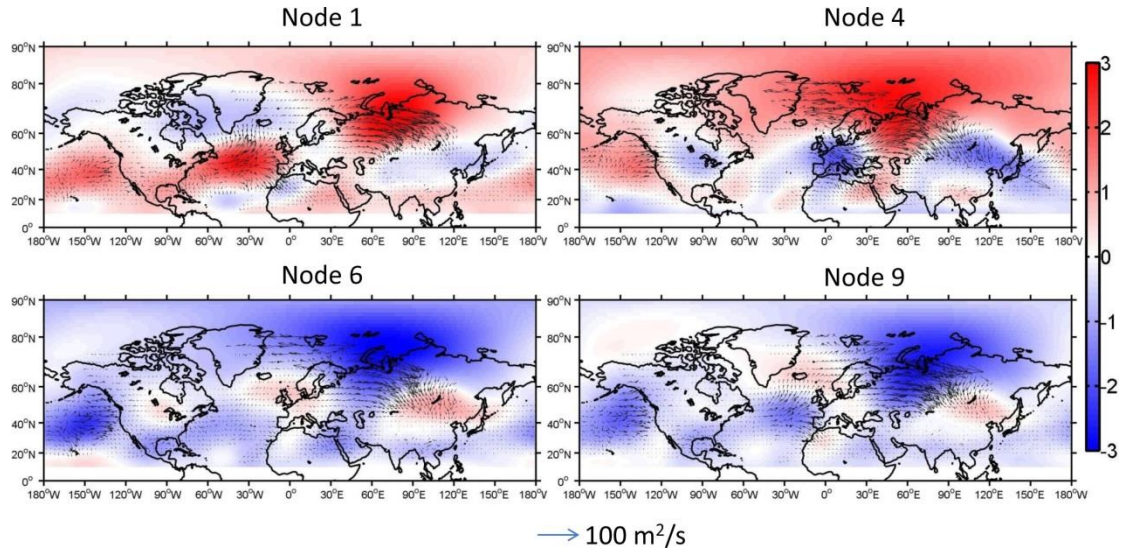


1407  
1408  
1409  
1410  
1411  
1412  
1413  
1414  
1415  
1416  
1417  
1418

Figure 11. Anomalous 500-hPa geopotential height (gpm) regressed into the normalized time series of occurrence number for nodes 1, 4, 6, and 9 without removing its linear trend from ERA-Interim reanalysis over the 1979-2019 period.

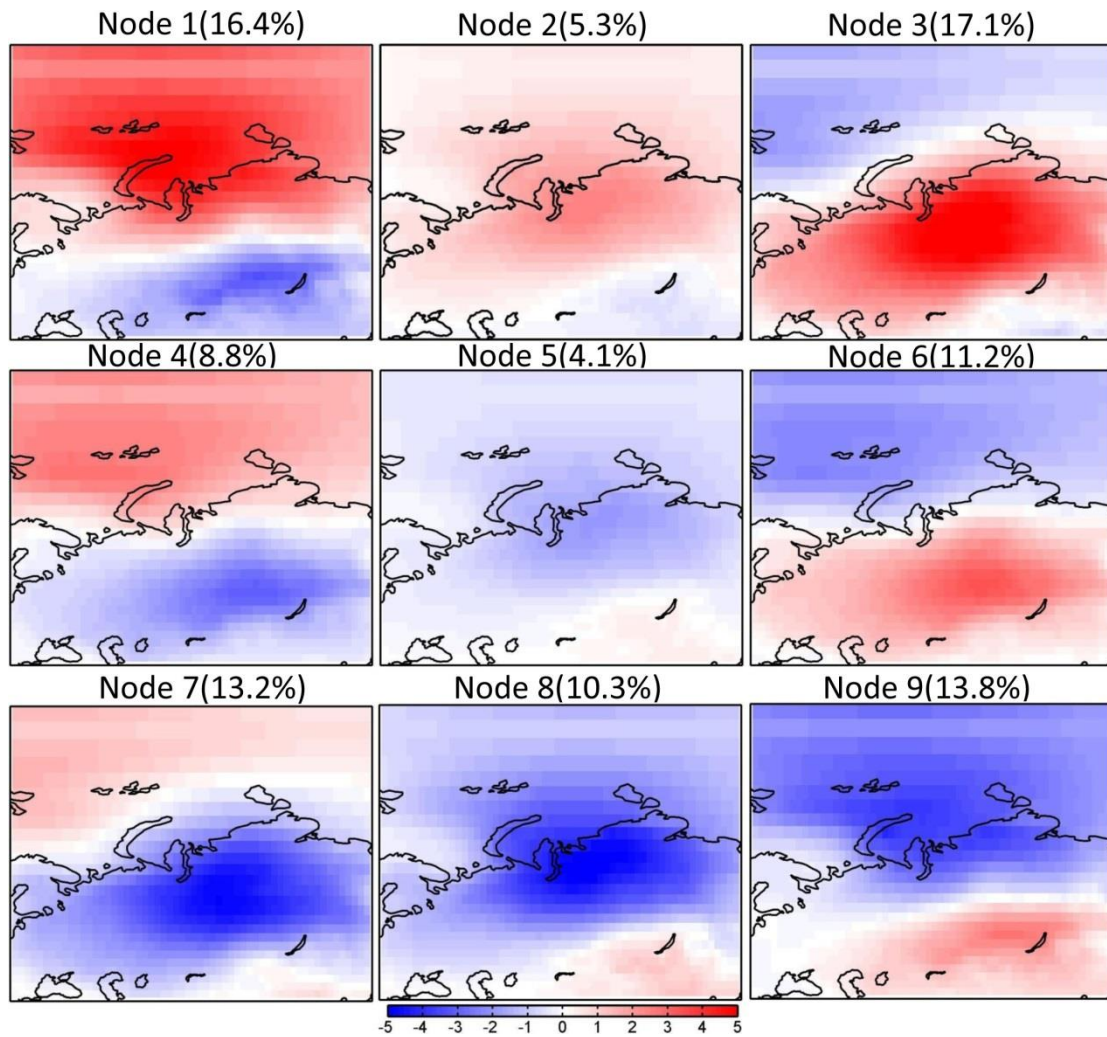


1419  
1420  
1421  
1422  
1423



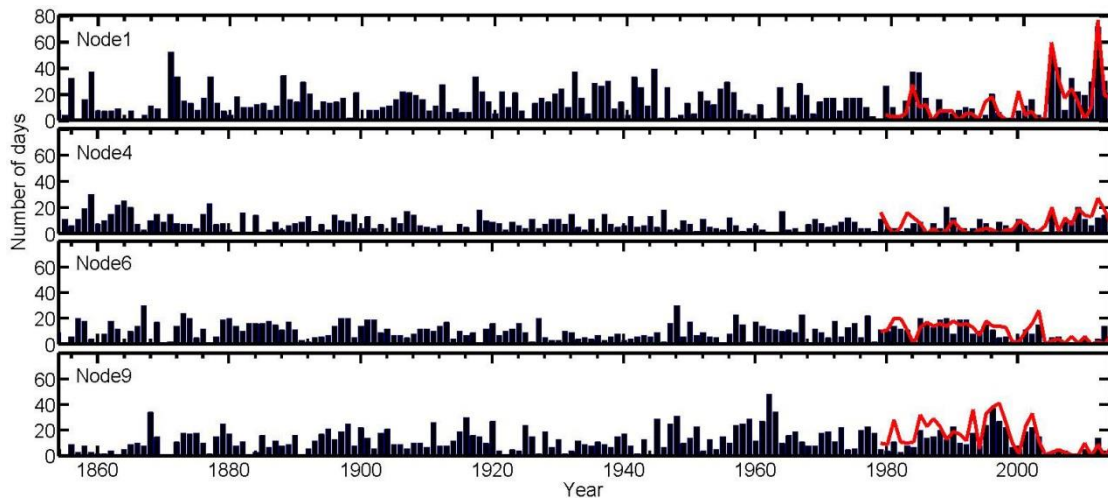
1424  
1425  
1426  
1427  
1428  
1429  
1430  
1431  
1432  
1433  
1434  
1435  
1436  
1437

Figure 12. The anomalous wave activity flux (vectors) (Takaya and Nakamura, 2001) and stream function (colors, units:  $10^7 \text{ m}^2/\text{s}^{-1}$ ) regressed onto the normalized time series of occurrence number for nodes 1, 4, 6, and 9 without removing their linear trends from ERA-Interim reanalysis over the 1979-2019 period.



1438  
 1439  
 1440  
 1441  
 1442  
 1443  
 1444  
 1445  
 1446  
 1447  
 1448  
 1449  
 1450  
 1451  
 1452  
 1453  
 1454  
 1455  
 1456  
 1457  
 1458

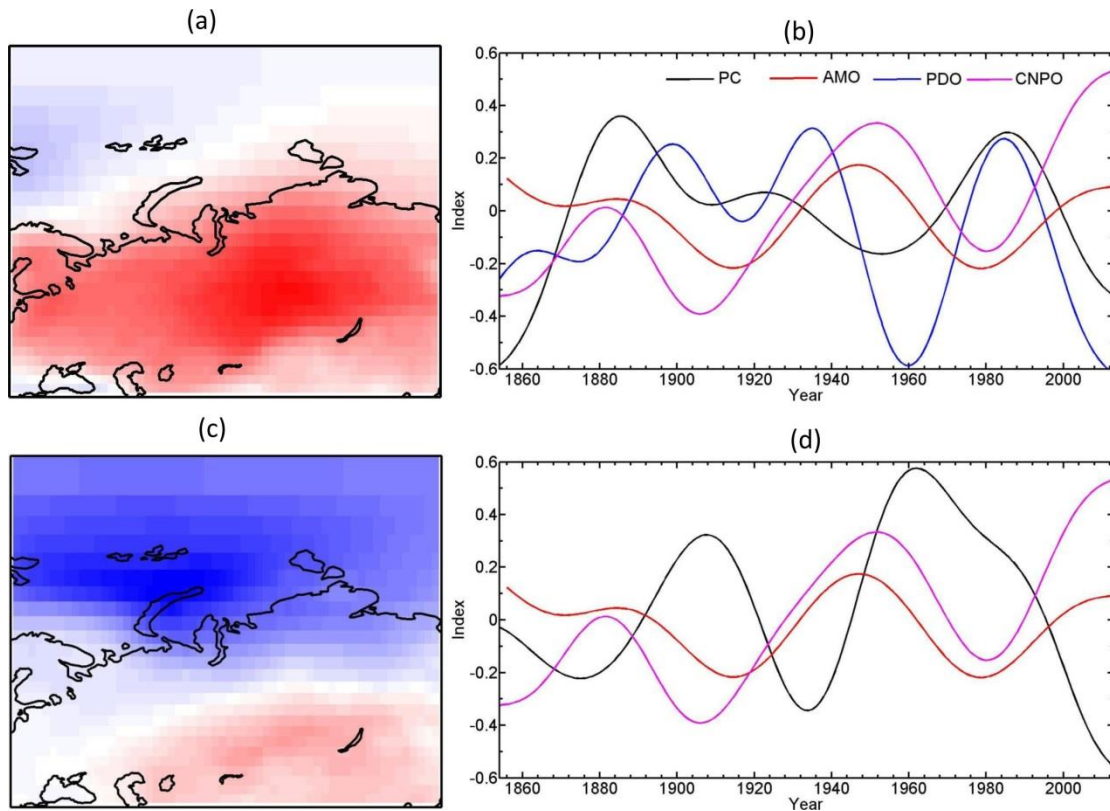
Figure 13. Spatial patterns of SOM nodes for detrended daily wintertime (December, January, and February) surface air temperature anomalies (°C) from the 20CR reanalysis for the 1851-2014 period. The number in brackets denotes the frequency of the occurrence for each node.



1459  
 1460  
 1461  
 1462  
 1463  
 1464  
 1465  
 1466  
 1467  
 1468  
 1469  
 1470  
 1471  
 1472  
 1473  
 1474  
 1475  
 1476  
 1477  
 1478  
 1479  
 1480  
 1481  
 1482  
 1483  
 1484  
 1485  
 1486  
 1487  
 1488  
 1489  
 1490  
 1491

Figure 14. Time series of the number of days for occurrence of each SOM node in Figure 13 from the 20CR reanalysis for the 1851-2014 period. The thick red lines denote the result in Figure 7 from the ERA-Interim reanalysis for the 1979-2019 period.

1492  
1493



1494

1495 Figure 15. The (a) leading pattern and (b) its time series (PC1 and PC2) of EOF analysis of  
1496 wintertime surface air temperature anomalies [from the 20CR reanalysis for the 1851-2014 period.](#)  
1497 Prior to EOF analysis, surface air temperature data are detrended. A 40-yr low-pass filter is  
1498 applied to the time series of PC1, PC2, AMO, PDO, and central North Pacific Ocean (CNPO)  
1499 indices. The correlation coefficients between PC1 and AMO, PDO and CNPO indices are -0.46  
1500 ( $p < 0.0001$ ), 0.38 ( $p < 0.0001$ ), and -0.19 ( $p = 0.019$ ); those between PC2 and  
1501 AMO, PDO and CNPO indices are -0.44 ( $p < 0.0001$ ), 0.38 ( $p < 0.0001$ ), and -0.26 ( $p = 0.0009$ ).

1502